The Journal of Neuroscience, July 1991, 11(7): 1959–1979

A Detailed Model of the Primary Visual Pathway in the Cat: Comparison of Afferent Excitatory and Intracortical Inhibitory Connection Schemes for Orientation Selectivity

Florentin Wörgötter[a] and Christof Koch

Computation and Neural Systems Program, California Institute of Technology, Pasadena, California 91125

In order to arrive at a quantitative understanding of the dynamics of cortical neuronal networks, we simulated a detailed model of the primary visual pathway of the adult cat. This computer model comprises a 5° × 5° patch of the visual field at a retinal eccentricity of 4.5° and includes 2048 ON- and OFF-center retinal β-ganglion cells, 8192 geniculate X-cells, and 4096 simple cells in layer IV in area 17. The neurons are implemented as improved integrate-and-fire units. Cortical receptive fields are determined by the pattern of afferent convergence and by inhibitory intracortical connections. Orientation columns are implemented continuously with a realistic receptive field scatter and jitter in the preferred orientations.

We first show that realistic ON–OFF-responses, orientation selectivity, velocity low-pass behavior, null response, and responses to spot stimuli can be obtained with an appropriate alignment of geniculate neurons converging onto the cortical simple cell (Hubel and Wiesel, 1962) and in the absence of intracortical connections. However, the average receptive field elongation (length to width) required to obtain realistic orientation tuning is 4.0, much higher than the average observed elongation. This strongly argues for additional intracortical mechanisms sharpening orientation selectivity.

In the second stage, we simulated five different inhibitory intracortical connection patterns (random, local, sparse-local, circular, and cross-orientation) in order to investigate the connection specificity necessary to achieve orientation tuning. Inhibitory connection schemes were superimposed onto Hubel and Wiesel–type receptive fields with an elongation of 1.78. Cross-orientation inhibition gave rise to different horizontal and vertical orientation tuning curves, something not observed experimentally. A combination of two inhibitory schemes, local and circular inhibition (a weak form of cross-orientation inhibition), is in good agreement with observed receptive field properties. The specificity required to establish these connections during development is low. We propose that orientation selectivity is caused by at least three different mechanisms ("eclectic" model): a weak afferent geniculate bias, broadly tuned cross-orientation inhibition, and some iso-orientation inhibition.

The most surprising finding is that an isotropic connection scheme, circular inhibition, in which a cell inhibits all of its postsynaptic target cells at a distance of approximately 500 μm, enhances orientation tuning and leads to a significant directional bias. This is caused by the embedding of cortical cells within a columnar structure and does not depend on our specific assumptions. Thus, anisotropic behavior can arise from isotropic long-range connections, making it likely that directional tuning is to some extent dependent upon the establishment of orientation selectivity.

The visual system of vertebrates is one of the most elaborate information-processing systems known to man. Despite three decades of intensive research, there is still an amazingly high degree of disagreement on even the basic mechanisms underlying visual signal processing. One of the most salient differences between cells in visual cortex and their afferents in the LGN is that the former are much more particular about what they respond to. Thus, in order to fire cells in cat visual cortex, the visual stimulus, most commonly bars or gratings, must have a certain orientation and very often move in a specific direction, while LGN cells are largely insensitive to variations in these parameters. A number of models have attempted to account for the origin of this behavior. The first, and most influential, model for orientation selectivity was proposed almost 30 years ago (Hubel and Wiesel, 1962; referred to here as "HW model"). It postulated that orientation selectivity arises from an appropriate alignment of synaptic input from the LGN, such that geniculate cells whose receptive fields fall along a row excite a cortical cell. Alternative models have invoked orientation-selective geniculate cells (Vidyasagar, 1984, 1987; Shou and Leventhal, 1989) or, more commonly, the use of inhibition to shape orientation tuning (Benevento et al., 1972; Blakemore and Tobin, 1972; Bishop et al., 1973; Sillito, 1975, Braitenberg and Braitenberg, 1979; Sillito et al., 1980; Heggelund, 1981, 1986; Morrone et al., 1982; Orban, 1984; for a review, see Ferster and Koch, 1987). The majority of these models are related to so-called iso- and cross-orientation inhibition models. In its simplest form, iso-orientation inhibition requires one of two cortical cells with

Received May 16, 1990; revised Jan. 9, 1991; accepted Jan. 11, 1991.

This project could never have gotten off the ground without Udo Wehmeier's skills at writing software on various machines in various languages. Matt Wilson provided help in mutating an early version of the GENESIS software into a visual cortex model. David van Essen was the midwife in charge of biological realism at the birth of this computer cat. F.W. was supported by Deutsche Forschungsgemeinschaft Grant WO-388. C.K. acknowledges support from a National Science Foundation Presidential Young Investigator Award, by grants from the Air Force Office of Scientific Research and the James S. McDonnell Foundation, and by a Bioscience Grant for International Research from the New Energy and Industrial Technology Development Organization in Japan.

Correspondence should be addressed to Dr. Christof Koch, Division of Biology, 216-76, Caltech, Pasadena, CA 91125.

[a]Present address: Institute of Physiology, Ruhr University Bochum, D-4630 Bochum, Germany.

partially overlapping receptive field and similar orientation preference to inhibit the other cell. The inhibited cell will then fail to respond (or respond in a reduced manner) over that part of its receptive field where the overlap occurred. This reduces the width of its receptive field relative to the length, leading to enhanced orientation selectivity. In cross-orientation inhibition, inhibition originates from a cortical cell with spatially overlapping receptive field but orthogonal orientation preference. Any stimulus exciting the inhibitory cell then results in a reduction of the response to the nonpreferred orientation in the inhibited cell, thereby sharpening its orientation tuning.

At the current time, conflicting and contradictory electrophysiological as well as pharmacological evidence exists supporting one or the other class of models (for recent reviews, see Ferster and Koch, 1987; Martin, 1988). Some of the arguments favoring HW-like models are that simple cells receive powerful monosynaptic excitation from relay cells in the LGN (Ferster and Lindström, 1983), that EPSPs evoked by bars of light are strongly tuned for orientation, and that several properties of visually evoked EPSPs can be well fit by simple quantitative models based on the HW scheme (Ferster, 1986). Furthermore, the absence of nonoriented inhibitory interneurons in cat area 17 (as required by the standard iso-orientation scheme; Heggelund, 1981) and the absence of intracellular IPSPs during stimulation in the nonoptimal orientation (Ferster, 1987; Douglas et al., 1988; Koch et al., 1990; but see Creutzfeldt et al., 1974) argue against cross-orientation inhibition.

Evidence favoring inhibitory schemes is provided by experiments in which the action of the principal cortical inhibitory neurotransmitter, GABA, is blocked by application of bicuculline and other GABA antagonists (Sillito, 1975, 1977, 1979; Tsumoto et al., 1979; Sillito et al., 1980; Wolf et al., 1986). This leads to a reduction or to a loss of orientation and direction selectivity in about half of all simple cells. Elevating the activity of the cortical cell by using a conditioning stimulus at the optimal orientation (Bishop et al., 1973; Morrone et al., 1982) or by excitatory amino acids (Hess and Murata, 1974; Ramoa et al., 1986) reveals the suppressive effects of a test stimulus at the nonoptimal orientation. Furthermore, inactivating small amounts of cortical tissue by iontophoretic application of GABA at distances of 0.5–1.5 mm from the cortical cell under investigation reveals loss of orientation tuning, arguing for additional cortical mechanisms contributing towards orientation selectivity (F. Wörgötter and U. T. Eysel, unpublished observations). Cross-correlation analysis reveals inhibitory interconnections among cells with different but not orthogonal orientation preferences (Hata et al., 1988). Another fact in disagreement with a purely HW model is that the orientation tuning of simple cells is only weakly correlated with their width-to-length aspect ratio ($r = 0.47$; Watkins and Berkley, 1974). Finally, a purely feedforward HW model will fail to demonstrate significant amounts of gain control in response to changing contrast, different from inhibitory feedback models (Wehmeier et al., 1989). All these and many more arguments have been used in the debate about the origin of orientation selectivity. One way to resolve this apparent dilemma is to argue for an "eclectic" model, incorporating both geniculate afferents arranged in a row and cortical inhibition (Koch, 1987; see also Orban, 1984; Martin, 1988). Furthermore, all of the models discussed above neglect any contribution the excitatory corticocortical connections can make towards orientation tuning. Given the large fraction of excitatory synapses on a typical pyramidal cell originating from other cortical pyramidal cells, such a contribution could be vital to explain the properties of receptive fields (see, e.g., Douglas et al., 1989).

We believe that one way to cut the Gordian knot of the origin of orientation selectivity is via a detailed modeling approach, incorporating as much anatomical and electrophysiological data as possible. This will enable us to investigate the different models and will give us a quantitative assessment of which wiring schemes are consistent with the evidence at hand. It has been our experience that detailed simulations very often also reveal inconsistencies in the models not apparent upon mere reflection.

A small number of simple quantitative models have appeared over the years (e.g., Nielsen, 1983; Ferster, 1987; Soodak, 1987). The majority of these models have been restricted to single-cell receptive fields, and none have investigated the temporal dynamics of a population of interacting cortical neurons. The obvious advantage of such models lies in their tractability and in the transparency of the associated parameter ranges, while their disadvantage is the unrealistic assumptions inherent in these models (e.g., stationary nonlinearities, no cortical interactions, absence of jitter in receptive fields, etc.). The computational complexity and cost associated with investigating the detailed dynamics of realistic cortical networks with massive interactions, such as in our study or in that of Finkel and Edelman (1989; see also Wilson and Bower, 1989, and Traub et al., 1989, for similar complex models of olfactory cortex and hippocampus, respectively), make this endeavor much more difficult. Such simulations may contain hundreds of parameters! It is obvious that, with this degree of freedom, virtually every type of behavior can be generated. It thus becomes crucial for modelers to carefully constrain their parameters using available experimental data. If such data are missing or incomplete, as is usually the case, modelers should avoid the pitfall of demonstrating each and every known phenomenon by simply raising the level of complexity of the model. Instead, the burden of proof should be toward showing that no simpler structure can generate any particular behavior. This is the principal reason why large-scale brain models are only useful in answering well-defined questions if they are intended to go beyond a mere reproduction of existing data.

Even at a reduced level of complexity, both large-scale brain models and real cortex share at least one property: their overall system behavior is not readily understood in terms of the properties of individual components. Thus, because a large-scale search through the parameter space is prohibitively expensive, intelligent use must be made of a combination of analytical insight and numerical modeling. Another problem shared by modelers and experimentalists alike is how to study, analyze, and display the activity patterns of tens of thousands of neurons as they evolve over time (Wilson and Bower, 1989). We have resorted to using in our computer simulations exactly the same methods and conventions experimentalists use routinely when recording from animals: poststimulus time histograms (PSTHs), population responses, and tuning curves.

In the present paper, we describe how we modeled about 5° × 5° of the primary visual pathway of an adult cat. In a first step, we will demonstrate that several of the most prominent features of simple cells (e.g., ON- and OFF-subfields, velocity tuning, orientation selectivity) can be generated easily with only a few assumptions. In a second step, the model is used to investigate the involvement of inhibitory interactions of various types (e.g., random inhibition, iso-orientation inhibition, cross-

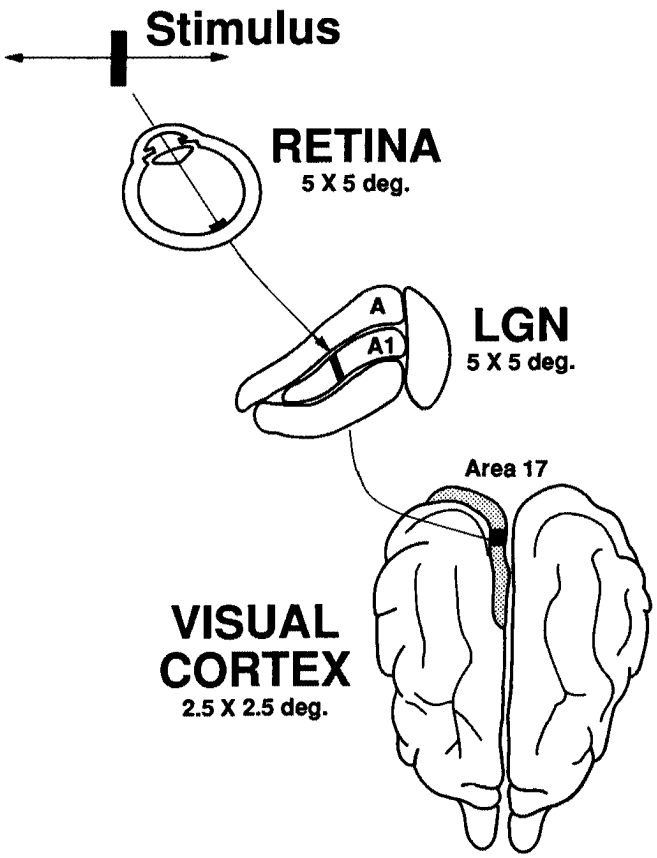

Figure 1. Schematic of the cortex model. A 5° × 5° patch of the retina is modeled at about 4.5° excentricity. Activity from this patch is passed through a corresponding region of the LGN into layer IV of area 17, where only a subset of 2.5° × 2.5° is simulated.

orientation inhibition). Certain conceptual problems will be revealed, and we will show that any single mechanism only produces realistic orientation selectivity within a small range of parameter values. The most intriguing finding demonstrates that a directional bias arises from isotropic cortical connections (circular inhibition).

Structure of the Model

The structure of the computer model used in this study is very similar to that described by Wehmeier et al. (1989), and we refer the interested reader to this didactic article for additional details of our computer implementation.

General outline

The model simulates parts of the early visual pathway of the adult cat. Thus, unless otherwise mentioned, all experimental data will refer to the adult cat. This animal was chosen in view of the considerable amount of anatomical and physiological data available in the literature. We simulate a monocular patch of 5° × 5° at a retinal eccentricity of 4.5°. Because the dominant input to area 17 in cat comprises X-geniculate cells (Sherman, 1985), we choose to simulate only ON- and OFF-retinal ganglion cells of the X-type, corresponding to the anatomical β-ganglion cell class (Boycott and Wässle, 1974). The projection of these cells was traced to the LGN and finally to the corresponding population of neurons in layer IV of the visual cortex. Figure 1 summarizes the basic topographical layout of the model.

Single-cell model

The simulated neurons exhibit realistic responses based on the determination of the changes in membrane potential computed from the spiking input each cell receives. Each cell is modeled as a single passive compartment with a capacitance, C_m, in parallel with a membrane leak conductance, g_{leak}, and a leak battery, E_{leak}. The passive time constant $\tau = C_m/g_{leak}$. Every synapse is described by a synaptic reversal potential (E_{ex} or E_{inh}, for excitatory and inhibitory synapses, respectively) in series with a transient conductance increase $g_{ex}(t)$ and $g_{inh}(t)$. The time course of these induced conductance changes follows an α function: $g(t) = \text{const} \cdot te^{-t/t_{peak}}$, with $t_{peak} = 1$ msec, const $= g_{peak}e^{+1/t_{peak}}$, and $g_{peak} = g(t_{peak})$. All synaptic input is added in parallel. The generation of action potentials is mimicked by a simple threshold; that is, at the time t_{spike} where $V_m(t)$ first exceeds the voltage threshold, V_{Thres}, an action potential is generated and relayed, with an appropriate delay, to all its postsynaptic cells. V_{Thres} varies from cell to cell, being uniformly distributed between −45 and −35 mV. An absolute and relative refractory period is modeled by a transient potassium conductance, $g_{AHP}(t)$, in series with a potassium reversal battery, $E_{AHP} = -90$ mV. Each time an action potential is generated, $g_{AHP}(t)$ becomes activated, leading to an afterhyperpolarization and preventing the cell from firing for a time dependent on the amplitude and time course of g_{AHP}. Different from the standard integrate-and-fire model, the cell's potential is not reset following the generation of an action potential, but continues to follow the dictates of its synaptic input and its internal current g_{AHP}. The equation describing the evolution of the state of every neuron is given by

$$C\frac{dV_m(t)}{dt} = \sum_{i=1}^{k} g_{ex}(t - t_i)(V_m(t) - E_{ex}) + \sum_{i=1}^{l} g_{inh}(t - t_i)(V_m(t) - E_{inh}) + g_{leak}(V_m(t) - E_{leak}) + g_{AHP}(t - t_{spike})(V_m(t) - E_{AHP}), \quad (1)$$

where C is the membrane capacitance; k and l are the total number of excitatory and inhibitory synapses; the t_i are the times of arrival of the appropriate action potential to that particular synapse; and t_{spike} is the time the cell generated an action potential. Notice that a propagation delay is incorporated into the times of arrival of action potentials, depending on the location of the pre- and the postsynaptic cell. The lower portion of Figure 2 shows the intracellular membrane potential of two different cortical cells. We choose realistic values for the cellular parameters (Table 1), without attempting to vary these numbers in any systematic way.

Retina

The simulated retina comprises a 2-D distribution of ON- and OFF-center β-ganglion cells with circular receptive fields, located on a noisy hexagonal grid. We modeled a 1-mm² patch of β-cells, 1 mm away from the area centralis, which includes 2 × 1024 cells (Peichl and Wässle, 1979). In terms of visual field coordinates, this represents a 5° × 5° field of view at 4.5° eccentricity (Bishop et al., 1962). The factor of 2 results from implementing the ON- and OFF-subsystem. We assume that the density of cells is constant across this 1-mm² retinal patch,

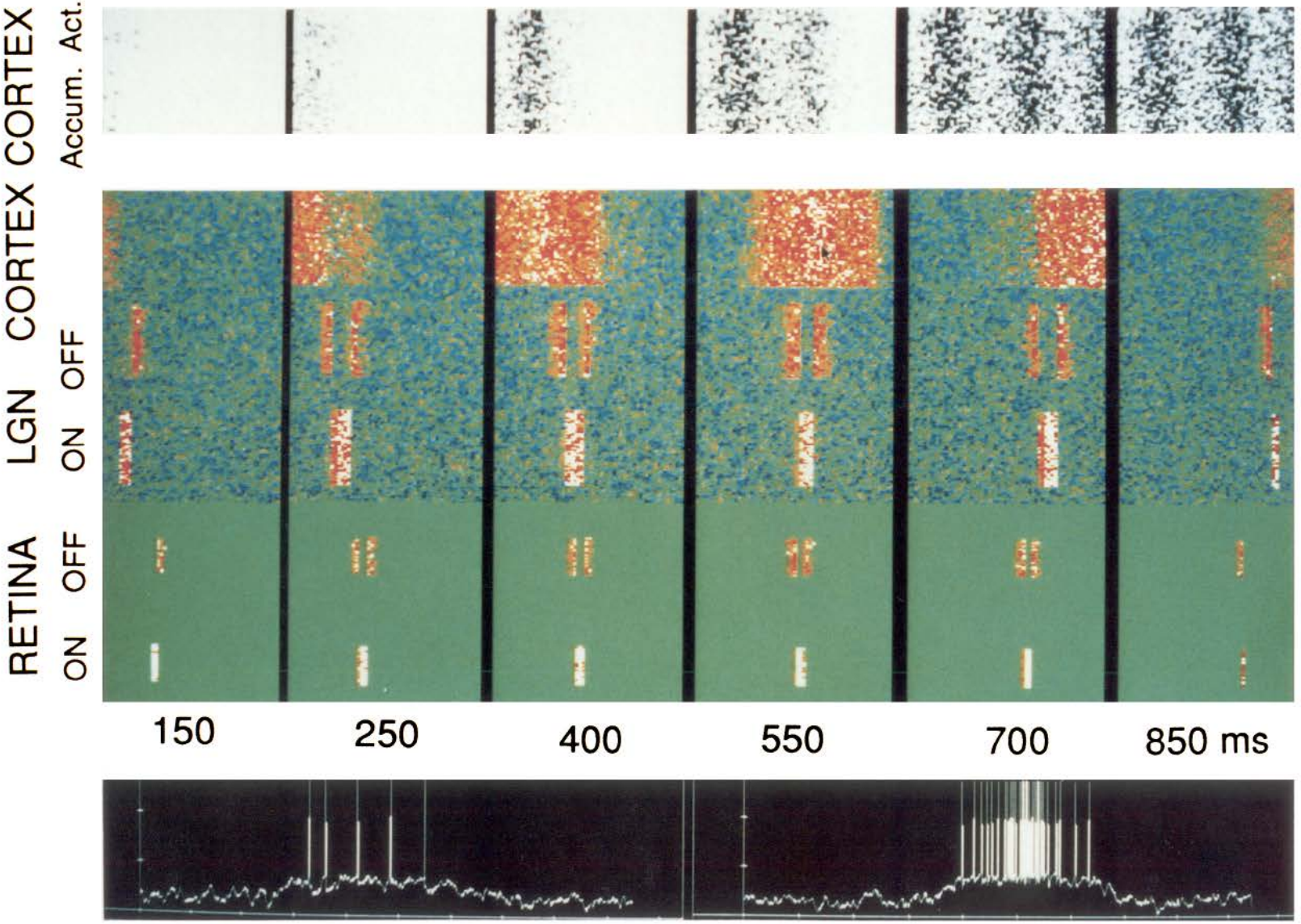

Figure 2. Run-time display of the cortex simulator. Each *small square* represents a single cell. A vertical-bar stimulus moves at a speed of 5°/sec from left to right across the simulated retinal patch. *Top,* Accumulated activity in the cortex. The size of the *solid squares* represents the total number of action potentials accumulated by that particular cell up to the time indicated. At the end of the stimulus sweep, 2.5 hypercolumns can be clearly observed.Note that the overall activity has been artificially raised to yield clear orientation columns following a single stimulus sweep. *Middle,* Membrane potential of the five neuronal populations: ON– and OFF–β-type retinal ganglion cells, ON- and OFF-geniculate relay cells, and cortical simple cells. The *color* of each square represents the intracellular potential of that cell. *Warm colors* represent depolarization, and *darker blue* represents hyperpolarization; the resting potential is shown in *green*. Spikes appear in *white*. Small random fluctuations of the membrane potential have been included in cortical and geniculate but not in retinal cells. The response in the retina appears to be shifted compared to the LGN; this is due to the fact that 32 × 32 retinal cells project to 64 × 64 LGN cells. For graphical reasons, the retinal cell population has been centered, so that the outer parts of the retina contain, in fact, no cells at all. *Bottom,* Intracellular potential of two cortical simple cells in a horizontal and a vertical orientation column. The hyperpolarizing potentials seen are solely caused by the afterhyperpolarization following action potential discharge (g_{AHP}), because no inhibitory intracortical inhibition was included in this particular run.

Table 1. Parameters for geniculate and cortical cells

Symbol	Parameter	LGN	Cortex
C	Membrane capacitance	1 nF	2 nF
g_{leak}	Leakage conductance	0.1 μS	0.1 μS
E_{leak}	Leakage reversal potential	−71 mV	−71.0 mV
g_{ex}	Peak excitatory conductance (g_{peak})	0.15 μS	0.011 μS
E_{ex}	Excitatory synaptic reversal potential	20 mV	20.0 mV
g_{inh}	Peak inhibitory conductance (g_{peak})	—	0.055 μS
E_{inh}	Inhibitory synaptic reversal potential	—	−71.0 mV
g_{AHP}	Peak afterhyperpolarization conductance (g_{peak})	0.59 μS	0.59 μS

corresponding to about 16.5′ (minutes of arc) average distance between the cells on a hexagonal grid. We assume that the receptive fields of retinal ganglion cells are linear and separable in space and time (for a discussion, see Dawis et al., 1984). That is, their response to an arbitrary intensity distribution $I(x, y, t)$ can be described by

$$r(x, y, t) = \int_0^t \int_{-\infty}^{+\infty} \int_{-\infty}^{+\infty} G(x', y')L(t')I(x - x', y - y', t - t')\,dx'\,dy'\,dt', \tag{2}$$

where $G(x, y)$ is the spatial receptive field, and $L(t)$, its temporal impulse response function. Following Rodieck (1965) and Enroth-Cugell and Robson (1966), we use the difference of two Gaussians (DOG) to describe the spatial receptive field

$$G(x, y) = G_{center}(x, y) - G_{surround}(x, y), \tag{3}$$

with

$$G(x, y) = (K/2\pi\sigma^2)\exp[-(x^2 + y^2)/2\sigma^2]. \tag{4}$$

We use center and surround values for K and σ as measured by Linsenmeier et al. (1982): $\sigma_{center} = 10.6'$, $\sigma_{surround} = 31.8'$ (corresponding to a center width of 30′; Peichl and Wässle, 1979), and $K_{center}/K_{surround} = 17/16$. The numerical evaluation of the Gaussian kernel is terminated at $2\sigma_{surround}$. Thus, outside of this range, $G(x, y) = 0$. The temporal response associated with each Gaussian is that of a first-order low-pass filter:

$$L = e^{-t/\tau}/\tau \tag{5}$$

with $\tau_{center} = 10$ msec and $\tau_{surround} = 20$ msec (Richter and Ullman, 1982). Subtracting these two responses results in a transient, band-pass–like behavior, in good agreement with the known temporal response of retinal X-cells. We include a delay of $\delta t = 3$ msec between the center and the surround response (Enroth-Cugell et al., 1983). The response of an individual cell is then given by

$$R(x, y, t) = r_{center}(x, y, t) - r_{surround}(x, y, t - \delta t). \tag{6}$$

At every point on the hexagonal lattice, the positive part of $R(x, y, t)$ is carried by an ON-center and OFF-surround cell (termed an ON-cell), while the negative part of R is carried by an OFF-center and ON-surround cell (OFF-cell). Binary action potentials are generated from this continuous response function by a Poisson process. The probability that the ganglion cell fires an action potential in the small interval between t and $t + \Delta t$ (with $\Delta t \ll 1$) is given by

$$p(x, y, t) = p_0 \cdot \Delta t \cdot R(x, y, t), \tag{7}$$

where p_0 is an appropriate normalization constant. We simulate the effect of varying the visual contrast of the stimulus by varying p_0. Our model retina results in realistic responses to visual stimulation (for several examples, see Wehmeier et al., 1989), entirely sufficient to investigate cortical activity patterns.

Lateral geniculate nucleus

The major projection from the retina leads to the lateral geniculate nucleus (LGN). With few exceptions, each geniculate cell seems to receive its innervation from a single or a few retinal ganglion cells of the same class, and the response properties of these geniculate neurons are essentially the same as those of their retinal counterparts (Hubel and Wiesel, 1961; Singer and Creutzfeldt, 1970). Retinal X-ganglion cells project mainly into the A and A1 layers of the LGN. Of the approximately 450,000 cells in the LGN (Sanderson, 1971), two-thirds are located in the A and A1 layers, and about two-thirds of these are of the X-type. Thus, on average, each retinal X ON-center ganglion cell from one eye innervates three to four geniculate relay cells. In our model, we assume that each retinal cell projects onto four neighboring geniculate cells. Thus, the 2048 retinal cells project onto 8192 LGN cells, subdivided into ON- and OFF-cells, representing about 5° × 5° in the visual field. The projection is strictly topographic and preserves the spatial structure of the input image. Axonal propagation delays between retina and LGN were set between 3 and 4 msec. The current version of our model neglects the contrast sharpening that occurs in the LGN, due to inhibitory interactions (Hubel and Wiesel, 1961; Cleland et al., 1983; Shapley and Lennie, 1985; Eysel et al., 1986, 1987). The time constant of geniculate cells is set at 10 msec (Bloomfield et al., 1987).

Visual cortex

Topography and cell numbers

Layer IV in area 17 is the primary target for projections from the LGN. The model assumes that the X-cell projections from the LGN terminate in the lower part of layer IV, where the average cell density is 14,000 cells/mm² (Beaulieu and Colonnier, 1983). Because in this aspect of our study we are only concerned with inhibitory corticocortical interactions, we only model inhibitory GABAergic neurons in area 17. These cells make up about 20–25% of all cells (Tömböl, 1974; Winfield et al., 1980; Gabott and Somogyi, 1986). We do not distinguish between different anatomical subtypes. At the chosen eccentricity of 4.5° from the area centralis, the cortical magnification factor is about 1.0 mm per degree (Tusa et al., 1978). In order

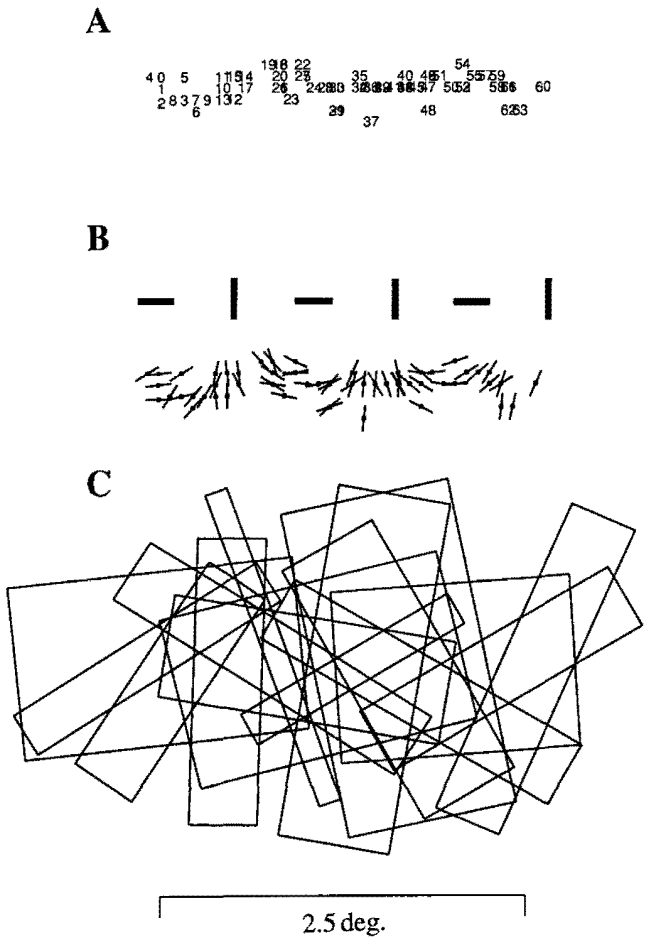

Figure 3. Topographical arrangement of the afferent projections from LGN to cortex. A cortical cell consists of one to four alternating ON- and OFF-subfields, each of which receives on average input from three columns and 23 rows of equidistantly spaced LGN cells (HW-type receptive field). *A,* Locations of the center of the HW-type receptive fields for one row of 64 cortical cells corresponding to 2.5°. Average receptive field scatter of about 200 μm can be seen. *Numbers* from 0 to 63 indicate the relative position of neurons (going from left to right). *B,* Preferred orientations of the cells showing the jitter in the orientation columns. The ideal column structure is depicted *above. C,* Plotting the outline of the receptive field of every fourth cell.

to avoid boundary effects, we only simulated the projection of the central 2.5° × 2.5° onto 2.5 × 2.5 mm of cortical tissue. This amounts to 17,500 cortical inhibitory neurons. To decrease computation time, we only simulated about one-fourth of all these cells, 4096 in total.

The projection from LGN to cortex preserves the topography of the visual field (Bilge et al., 1967; Tusa et al., 1978) but maps it approximately logarithmically (Fischer, 1973; Schwartz, 1977). At the chosen eccentricity, and taking into account that only a cortical patch subserving 2.5° × 2.5° of the visual field is simulated, we can well approximate this by a constant mapping. Although topography is preserved, the receptive field scatter in the cortex prevents accurate prediction of the actual spatial relationship between two receptive fields if the distance between the cells is less than 200 μm (Albus, 1975a,b). This is shown by plotting the receptive field centers of one row of 64 cortical cells in Figure 3*A*.

The divergence from LGN to cortex was assumed to be about 220; that is, a single LGN cell projects to about 220 cortical cells (Wehmeier et al., 1989). Each geniculate X-cell projects onto a circular patch of 0.72 mm² of cortex (Humphrey et al., 1985). The axonal propagation delay of the geniculate–cortex pathway is set to 5 msec with some random variations (Hoffmann et al., 1972). Small random fluctuations of the membrane potential were introduced into all cortical cells, leading to spontaneous background firing at frequencies between 0.05 and 2 Hz. The time constant of all cortical cells was set to 20 msec (Stratford et al., 1989).

Basic connection pattern for the generation of cortical receptive fields

One of the most prominent features of cortical simple cells is their specificity for oriented stimuli that goes in parallel with the elongated shape of their receptive fields. The ratios of width to length of their receptive fields range from 1:5 (very elongated) to 1:1 (round; Watkins and Berkley, 1974; Gilbert, 1977; Jones and Palmer, 1987). The basic mechanism that we implemented in most of our simulations relies on input from aligned receptive fields from the LGN (Hubel and Wiesel, 1962). This type of connection we will call the HW type.

Simple-cell receptive fields consist of multiple non- or sparsely overlapping ON- and OFF-subfields. From one up to four subfields have been implemented in the model, the sizes of the subfields being constant for each cell. A Gaussian probability distribution determined the actual number of subfields for each cell such that cells with two or three subfields predominate. The average number of rows and columns of LGN cells that form a subfield is fixed (see below); the actual numbers for individual cells varied with a Gaussian probability distribution allowing for deviations from the average of about ±4 for the subfield length and ±2 for its width.

In the following, we proceed in two stages. We first try to mimic as much of the cortical behavior as possible *without* intracortical inhibition, while we assess the contribution of intracortical inhibition toward orientation selectivity in the second stage.

Orientation tuning in the absence of intracortical inhibition can only be achieved with a rather large ratio of length to width (called *aspect ratio*) of the HW-type receptive field. Thus, for the first stage, an average aspect ratio of 23 × 3 LGN cells was assumed for each cortical subfield, and the examples shown in the following refer to these values. Figure 4 illustrates how the LGN input for a typical cell in the cortex is arranged to produce an ON–OFF- and an OFF–ON–OFF-type receptive field. Each small rectangle in the diagram represents the center of an individual LGN cell. ON (or OFF, respectively) subfields receive only input from ON-center (or OFF-center, respectively) LGN cells (Tanaka, 1983). The actual structure of the receptive field is illustrated on the right side of the panels, generated by superimposing DOGs according to the spatial arrangement shown to the left. For graphical reasons, OFF-responses are plotted as negative values. They are not to be confused with inhibition. The average topological distance between two adjacent LGN cells is about 0.08°. Because the receptive field size of the center of a retinal or LGN cell is 0.5°, the aspect ratio of a 23 × 3 cell arrangement (Fig. 4*B*) corresponds to a subfield elongation of 3.2. Incorporating intracortical inhibition allows us to reduce the average aspect ratio to 13 × 5 LGN cells, corresponding to an elongation of about 1.8. Note that orientation tuning is directly influenced by the aspect ratio of cortical subfields. For

instance, two receptive fields with the same total aspect ratio will have different orientation tuning if one has two, and the other, three subfields. Therefore, all aspect ratios given in this study refer to subfields (Daugman, 1980, 1984).

Orientation-selective cells in the visual cortex are arranged in orientation columns (Hubel and Wiesel, 1963). A set of columns containing all orientation preferences, a hypercolumn, has a width of 0.7–1.2 mm (Albus, 1975b). In our model, orientation columns were implemented using an HW type of connection pattern for the basic determination of orientation preference. The orientation in the columns varies continuously, with a spatial periodicity of 1.0 mm. We therefore implemented about 2.5 hypercolumns (starting with orientation preference for vertical stimuli). The columns are vertically arranged; that is, they are running straight from top to bottom in the cortical patch. This approximation of a more realistic bent cortical column structure is valid over distances of about 1.5 mm (Albus, 1975b), more than half of our simulated patch. Within one of our columns, orientation preference is constant with a Gaussian distribution of jitter averaging 10° (Albus, 1975b). Figure 3*B* shows the orientation preferences for the same row of cortical cells as in Figure 3*A*; the idealized column structure is depicted above. The actual outline of the receptive fields is shown for a quarter of the cells (16) in Figure 3*C*.

The propagation of action potentials among cortical cells includes a delay. The value of this delay was drawn from a Gaussian distribution around a mean value determined by the axonal propagation velocity (which varied between 0.5 and 2 m/sec) and the geometrical distance between the pre- and the postsynaptic cell.

Computer implementation

The simulations were carried out on SUN-4 UNIX-based workstations. The program, written in C, was developed by U. Wehmeier (see Wehmeier et al., 1989) and derived initially from GENESIS, the Caltech-based neural network simulator (Wilson and Bower, 1989). The cellular potential was updated using a first-order backward Euler numerical procedure. Computational efficiency was a major issue. In some of the cases incorporating massive inhibitory feedback, up to 3.5 million synapses were being simulated. In such a case, our SUN workstation simulated 1000 msec of real time in about 5 hr computer time (a slowing down of 18,000). This obviously places serious limits on our ability to explore large parameter variations. We are now porting our code onto the massively parallel Connection Machine CM-2 and have achieved speedups of about 100 in our initial trials.

Visual stimuli

The intensity function $I(x, y, t)$ usually corresponds to that of an elongated and moving bar with a width of 0.5° and a length of more than 4.0° (e.g., Fig. 2). We also used moving spots (0.2° × 0.2°) or counterphasing sine-wave gratings. The contrast of all stimuli was usually held fixed at an arbitrary level. The actual contrast level is irrelevant because the level of neuronal activity reached at a given contrast level can be adjusted by varying the cellular parameters. For dark-bar stimuli, the same contrast level was used, but with an inverted sign.

Data analysis

In order to facilitate the direct comparison of our model with experimental data, we performed most of our data analysis in the same manner as our experimental colleagues. We generated

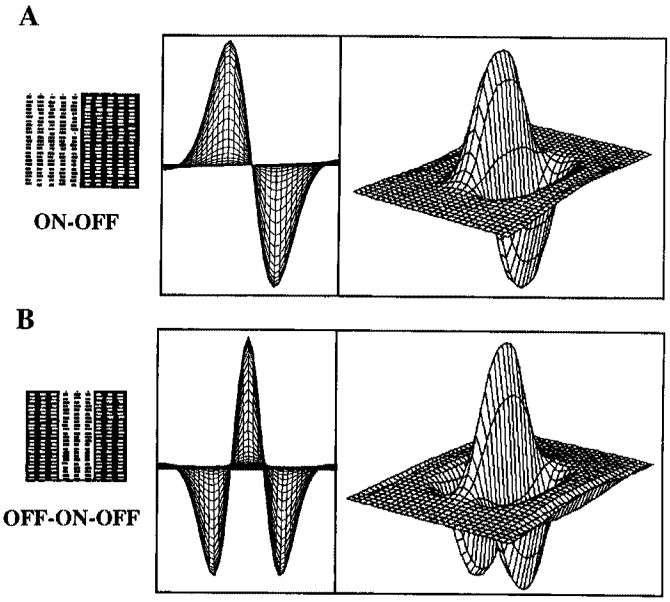

Figure 4. Typical receptive fields of cortical cells determined only by HW-type connections. *Left,* Schematic plot of the receptive field. Each *small rectangle* represents the center of an LGN cell. Different *sizes* encode the different axonal delays. *Middle* and *right,* Three-dimensional receptive field plots obtained by superimposing DOGs centered on the location of the LGN cells with positive (ON) and negative (OFF) sign and appropriate weights. *A,* Antisymmetic receptive field with ON–OFF-substructure. *B,* Symmetric receptive field with OFF–ON–OFF-substructure.

stimulus-locked poststimulus time histograms (PSTHs) and displayed orientation tuning curves in polar coordinates, plotting the peak response of each PSTH against the direction of stimulus motion. We also show in most cases average polar plots, obtained from 55 cells randomly selected from the central part of the simulated cortical patch in order to avoid boundary effects. All individual tuning curves were rotated prior to averaging so that the strongest response fell onto the 0° vector of the polar plot.

Directional and orientation tuning of a response was extracted from the polar plots by SDO analysis (Wörgötter and Eysel, 1987; Wörgötter et al., 1990). This method amounts to a discrete Fourier analysis of the maximum firing rate $f(\alpha)$ obtained by moving an elongated bar with orientation α across the receptive field. The angle α is then systematically varied from 0° to 360°. $f(\alpha)$ can then be represented as

$$f(\alpha) = A_0 + \sum_{n=1}^{\infty} [A_n \cos(n\alpha) + B_n \sin(n\alpha)]. \quad (8)$$

We can write down the following expressions for the amplitude and the phase of the nth component:

$$G_n = \sqrt{A_n^2 + B_n^2}, \quad (9)$$

$$\phi_n = \arctan(B_n/A_n). \quad (10)$$

The zeroth-order component, A_0, describes the mean peak response rate for all directions of movement; thus, it reflects the average sensitivity of the cell to unspecific stimulation and can be used as a measure of the general excitability of a cell on which all specific directional and orientational modulations are superimposed. The first harmonic (A_1 and B_1) is regarded as the

directional (D) component, and the second harmonic (A_2 and B_2) as the orientational (O) component of the response $f(\alpha)$. These components directly reflect the periodicity of direction (360°) and orientation (180°) in the visual field. The associated amplitude values, G_n as defined in Equation (9), define the tuning strength of the directional and orientational components, whereas the phases ϕ_n represent the preferred direction (PD) and preferred orientation (PO). We use normalized values of the amplitude to compensate for a mere shrinkage or expansion of the polar plot. Thus, we define $D = G_1/G_0 = (A_1^2 + B_1^2)^{1/2}/A_0$ and $O = G_2/G_0 = (A_2^2 + B_2^2)^{1/2}/A_0$. A_0 is usually given in impulses per second (I/sec), and PD and PO in degrees ($0° \leq PD < 360°$, $0° \leq PO < 180°$).

More commonly, the direction index (DI; the ratio of the response in the preferred direction minus the response in the null direction to the response in the preferred direction) and the width of the orientation tuning at half of the maximum value [half-width at half-height ($\theta_{1/2}$)] have been used to characterize cortical cells (Orban, 1984). Thus, for DI = 0, the cell is not direction selective, while DI ≈ 1 implies strong direction selectivity. These parameters can be related to those obtained from the SDO analysis using the following empirical relationships:

$$DI = 60.9 \log_{10}(D) - 38.7, \quad (11)$$

$$\theta_{1/2} = -63.1 \log_{10}(O) + 137.9. \quad (12)$$

The correlation r between these two sets of variables was found to be better than 0.85 in both cases. The rationale for these equations and a detailed comparison of the SDO analysis with the commonly used method are given elsewhere (Wörgötter et al., 1990). We believe that SDO analysis gives more reliable estimates of the direction and orientation tuning (Wörgötter et al., 1990). However, because this method is not widely used at the moment, we will supply DI (in %) and $\theta_{1/2}$ (in degrees) values in parentheses. Finally, most of our analysis is carried out on populations of cells, reflecting average cell properties.

Results

General features

The color plate (Fig. 2) illustrates a typical example of the performance of our model. In this simulation, only HW-type geniculocortical connections from a 23 × 3 array of geniculate cells have been included; no intracortical wiring has been incorporated. A vertical bright bar was swept at a speed of 5°/sec from left to right across the retina; each vertical slab in the figure corresponds to a snapshot at the time indicated. The state of the β-type retinal ganglion cells, as well as their geniculate and cortical counterparts, can be monitored throughout the simulation, each little square representing a single cell, and its color the cell's intracellular potential (for more details, see Fig. 2 caption). The stimulus enters the retinal patch in the leftmost time slice. Excitation in the retinal and geniculate OFF-populations travels ahead (as well as behind) of the ON-excitation, because OFF-center cells are ON-excited in their surround. The response of cortex to a vertical bar is not very specific, due to the lack of inhibitory interactions sharpening the orientation tuning. This can be seen best from the accumulated spike activity (top portion of Fig. 2). The size of the black squares scales with the number of spikes; by the end of the stimulation (rightmost panel), three darker and three lighter regions can be distinguished, representing columns with vertical or horizontal orientation preference (notice the smooth transition between columns). The intracellular recordings of two exemplar cells with horizontal and vertical preferred orientations are also illustrated. We refer the reader to Wehmeier et al. (1989) for more details concerning the response of retinal and geniculate cells to other stimuli.

ON–OFF-property and velocity tuning of cortical cells

Figure 5*A* shows the response of a cortical OFF–ON–OFF-cell to light- and dark-bar stimuli moving at 5°/sec. The same simulation parameters and only HW-type connections have been used as before. During stimulation with a dark bar, two separated peaks can be seen in the PSTH (lower panel in Fig. 5*A*). The light-bar stimulus reveals a single peak centered in the middle (upper panel in Fig. 5*A*).

The influence of stimulus velocity and of the degree of overlap between the ON- and OFF-subfields is further illustrated in Figure 5*B–G*. The upper row (Fig. 5*B,C*) shows that the apparent receptive field overlap is not influenced by the stimulus speed. The large degree of overlap between the ON- and OFF-response regions, as can be observed in the histogram, remains the same between 1°/sec and 5°/sec. We plotted the response of this cell as a function of the velocity of the bar in Figure 5*D*. It remains more or less flat for velocities up to 5–10°/sec and then drops off toward 0. The cell ceases to respond to a bar moving at 100°/sec. Without intracortical inhibition, such velocity "low-pass" behavior (Orban et al., 1981) is seen in all cells.

Figure 5*G* illustrates a band-pass–like velocity tuning curve with an optimum at a given velocity. This behavior was generated after including intracortical inhibition (local and circular; see below). Although the effects of intracortical inhibition will not be discussed until later, this result is shown here for reasons of comparison. According to the terminology of Orban et al. (1981), such a behavior is called "velocity tuned." It was found in about 12% of the cells.

The mean topographical distance between two adjacent LGN cells is about 0.08° in our simulation. Constructing a receptive field with the ON-subfield directly adjacent to the OFF-subfield leads to a rather large overlap between the ON- and the OFF-responses in the histograms (Fig. 5*A*). In real simple cells, subfields overlap to a much lesser extent. This could either be achieved by intracortical sideband inhibition or by a substantial degree of separation between the corresponding projections from the LGN. Figure 5, *E* and *F*, shows the overlap that arises from a separation of ON- and OFF-subfields by 0.16° (Fig. 5*E*) or by 0.24° (Fig. 5*F*), respectively. The overlap in the PSTH is decreased accordingly. However, even for the largest separation (Fig. 5*F*), an overlap of about 35% is still seen, due to the size of the LGN receptive fields.

X-cells in retina and LGN, and to a large extent, also simple cells in the visual cortex, display linear spatial summation. When stimulated with a counterphasing grating at a given spatial frequency, these cells will respond with an amplitude depending on the phase of the grating (i.e., its position on the receptive field). For these cells, there always exists at least one particular phase such that the influence arising from ON- and OFF-subfields will cancel out and the cell will cease to respond. This phenomenon has been called the null response and was observed in retinal X-cells (Hochstein and Shapley, 1976) and less pronounced in cortical simple cells (Movshon et al., 1978). Our model is able to reproduce this behavior. Figure 6 shows an example of an ON–OFF-cortical cell that was stimulated with a counterphased sine-wave grating of 1.5 cycles per degree. The

temporal period was 600 msec, and the grating was switched on at $t = 30$ msec. Eight histograms are shown, each representing a phase shift of 22.5° of the grating. At a relative phase shift of 0°, the cell stopped responding (null response). At phase shifts of ±90°, the responses are strongest. The phase shift between the −90° and the +90° histograms equals one-half of a spatial period; therefore, the onset of the response changes by half a period from the beginning to the middle of the histogram. Because at this stage of our model no intracortical inhibition is implemented and the output of all retinal and geniculate cells is half-wave rectified, the null response of our cortical cell is caused by all of the individual retinal cells having a null response to this particular stimulus. Thus, it ultimately arises from the linear ON- and OFF-responses that interact linearly within single retinal ganglion cells.

Responses to moving spots

Recently, Wörgötter and Eysel (1989) reported that the strongest response of cells in area 17 to a moving spot occurs if the spot travels along the long axis of the receptive field. This axis is orthogonal to the axis of preferred motion of a long bar. This response type was strongest in simple cells and is thought to be caused by temporal facilitation (Wörgötter and Holt, 1991). Thus, activity in one geniculate cell will excite its corresponding cortical target cell; the trace of this activity will persist for some time, dictated by the membrane time constants of all cells involved, and will facilitate the response of the cortical cell when the neighboring geniculate cell is activated. According to this analysis, HW-type connections should be sufficient to elicit this effect. Figure 7 shows the orientation tuning curves from three real and three simulated cells stimulated with a long bar (10°; Fig. 7*A,C*) and a small spot (0.2°; Fig. 7*B,D–F*. The cells in the upper part of the figure show pronounced responses to moving bars, with a vertical axis of preferred motion. The real simple cell shows strong directional tuning that is not seen in the simulation. The axis of preferred motion observed during spot stimulation is orthogonal to that for a bar, both for real and for simulated cells. The polar plots are normalized, but the response strength is significantly reduced for a moving spot and reaches only 30% of the value obtained with a moving bar of half the contrast. In several real cells, in particular in deep layers (Wörgötter and Eysel, 1989), unusual four-lobed polar plots have been observed during stimulation with a moving spot (e.g., Fig. 7*E*). This behavior is reproduced by the model, and cells with such a strange behavior are much more commonly observed in the simulation than in reality. This is probably due to missing intracortical inhibition at this stage of our simulation.

Varying inhibitory intracortical connections

The following section deals with the limitations in specificity that underlie different inhibitory corticocortical connection schemes. All simulations were performed with bright-bar stimuli. Because the cortical OFF-system is essentially silent (number of spikes in LGN-OFF/LGN-ON = 1/10) during these stimuli, we limited these simulations to only the ON-subsystem in retina, LGN, and cortex. Notice that no explicit attempt was made to incorporate direction-selective inhibitory wiring schemes.

Hubel and Wiesel wiring scheme

We have shown in the previous section that many cortical response types can be obtained when the model only includes

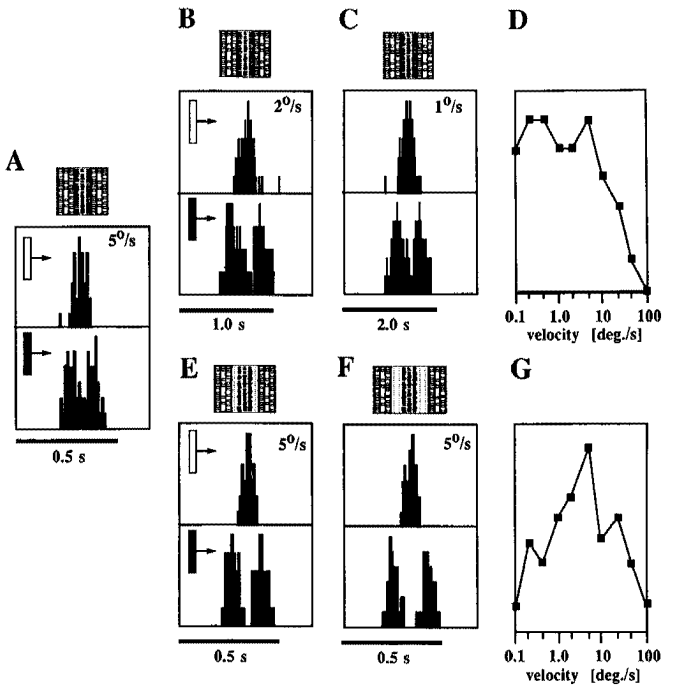

Figure 5. ON–OFF-characteristic, influence of stimulus speed, and subfield separation on the response of an even symmetric (OFF–ON–OFF) cell. The receptive field structure is shown *above* the panels. The *top* of each divided panel shows the response to a vertical light bar; the *bottom*, a dark bar. Stimulus speed: *A*, 5°/sec; *B*, 2°/sec; *C*, 1°/sec. *A–C*, Subfields remain not separated. Stimulus speed has no influence on the overlap of the histograms. *D*, Velocity response curve. A velocity low-pass behavior is observed. *E*, Stimulus speed 5°/sec subfield arrangement separated by 0.16°. *F*, Stimulus speed 5°/sec subfield arrangement separated by 0.24°. Even for the largest separation, about 35% overlap of the histograms is observed. *G*, Velocity response curve for another cortical cell after including intracortical inhibition. A velocity-tuned behavior is observed.

HW-type connections. However, the average ratio of receptive field length versus width needed to obtain realistic orientation tuning was 23 × 3 and therefore quite high. Figure 8 shows a comparison of the results obtained with different aspect ratios ranging from 9 × 7 to 31 × 3. Taking the size of LGN fields into account, these ratios correspond to cortical length : width ratios between 1.16 and 4.40. The top part of Figure 8 illustrates the cumulative population response of one hypercolumn to stimulation with a moving vertical bar. A clear distinction between the columns occurs only for the largest aspect ratio (31 × 3); smaller aspect ratios lead to substantially reduced orientation tuning. Little selectivity remains for a 9 × 7 receptive field. This effect can also be seen from the orientation tuning of an example cell (Fig. 8, middle row) and in the averaged polar plots shown below. The average O component equals only 9.5% ($\theta_{1/2} = 76.2°$) for the 9 × 7 aspect ratio and 18.6% (57.8°) for 13 × 5. The average O component in experimentally recorded simple cells is 75.0%, corresponding to a $\theta_{1/2}$ of 19.5° (Orban, 1984, his Table 7/1).

These values are being approached in the case of the 31 × 3 type of receptive fields, corresponding to an O value of 72.3% ($\phi_{1/2} = 20.6°$). As expected, the cells did not show any directional tuning, and the D components remained below 8.0%, corresponding to a DI of 16.3%.

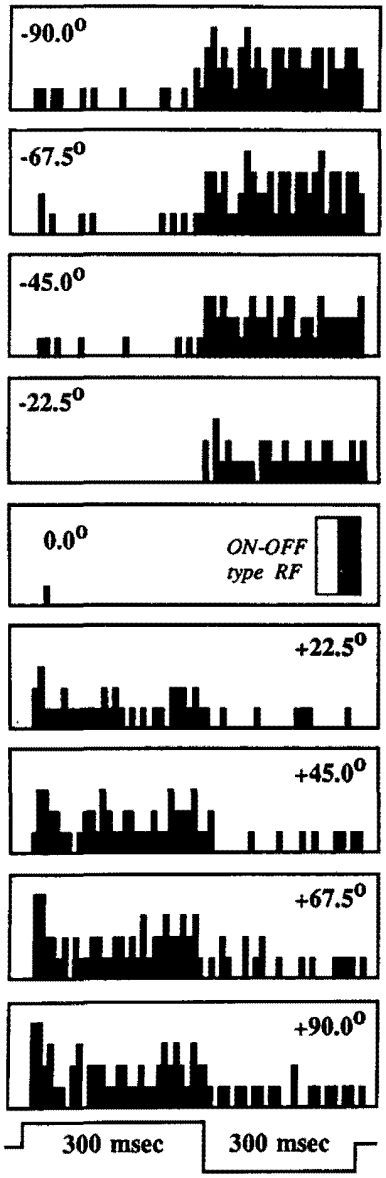

Figure 6. Cortical null response. A cortical cell with ON–OFF receptive field (RF) is stimulated with a counterphasing grating (1.5 cycles per degree) with a variable relative phase shift as indicated. The cell stops responding at 0° relative phase shift.

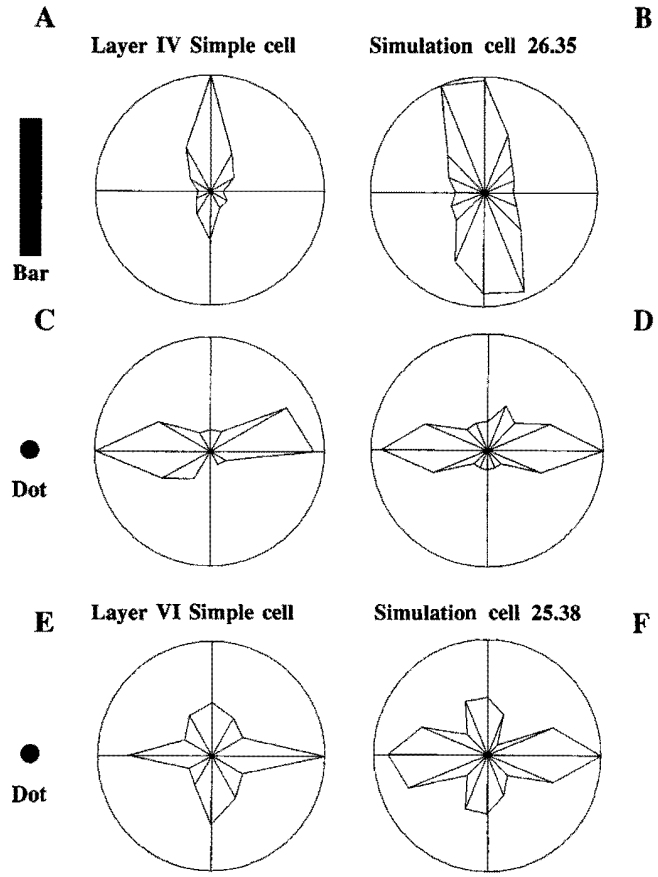

Figure 7. Responses to moving bars (*A, B*) and spots or dots (*C–F*). The *left side* shows the response of real cortical cells (modified from Wörgötter and Eysel, 1989, unpublished observations), and the *right side*, simulation results. *A–D*, The preferred axis of motion for a spot is orthogonal to that for a bar. *E* and *F*, Some cells show a superposition of the two orthogonal response components during stimulation with a spot. The simulation parameters are the same as in previous figures, except that twice the contrast value has been used for the spot.

Inhibitory wiring schemes

We assume that inhibitory intracortical wiring is superimposed onto an HW-like afferent orientation bias arising from an array of (on the average) 13 × 5 neighboring geniculate cells converging onto every cortical cell. As mentioned above, this corresponds to a receptive field width : length ratio of 1.78 and leads to a ϕ_{v_1} value of 57.8°.

We implemented two different types of connection schemes: long-range and short-range inhibition. The different topological relations that arise from long- and short-range inhibition, their relationship to the columnar organization, and the value of the associated axonal delays are all shown in Figure 9. All intracortical connection schemes are generated with the help of two different probability distributions. (1) The a priori probability determines whether or not the "topological requirements" between source and target cell are satisfied. The two most important such requirements are that no connections are made between two cells when their intracortical distance is either too large or too small (depending on the type of inhibition) or that no connections are established if the source cell appears under a certain angle with respect to the horizontal meridian. If the a priori probability is high enough, the two cells are potential candidates for a connection. Thus, this probability function encodes the specific type of inhibition used. (2) The a posteriori probability, a uniform distributed random number, will then decide if a potential connection (according to the a priori probability) is actually established.

The least specific long-range inhibitory connections are defined by *random* wiring (Fig. 9*A*). Here the probability of making a connection with the cell in the center is constant for all cells within the distance of half a hypercolumn, resulting in a disk-like structure of connected cells.

Circular inhibition (Fig. 9*B*) is more specific. Only cells at an approximate distance of half a hypercolumn are connected with high probability to the center cell. The resulting structure resembles an annulus. The a priori probability distribution has been chosen such that the annulus is about 200 μm wide. About 100 cells connect onto each target cell. *Partial circular* inhibition is closely related to cross-orientation inhibition (Morrone et al.,

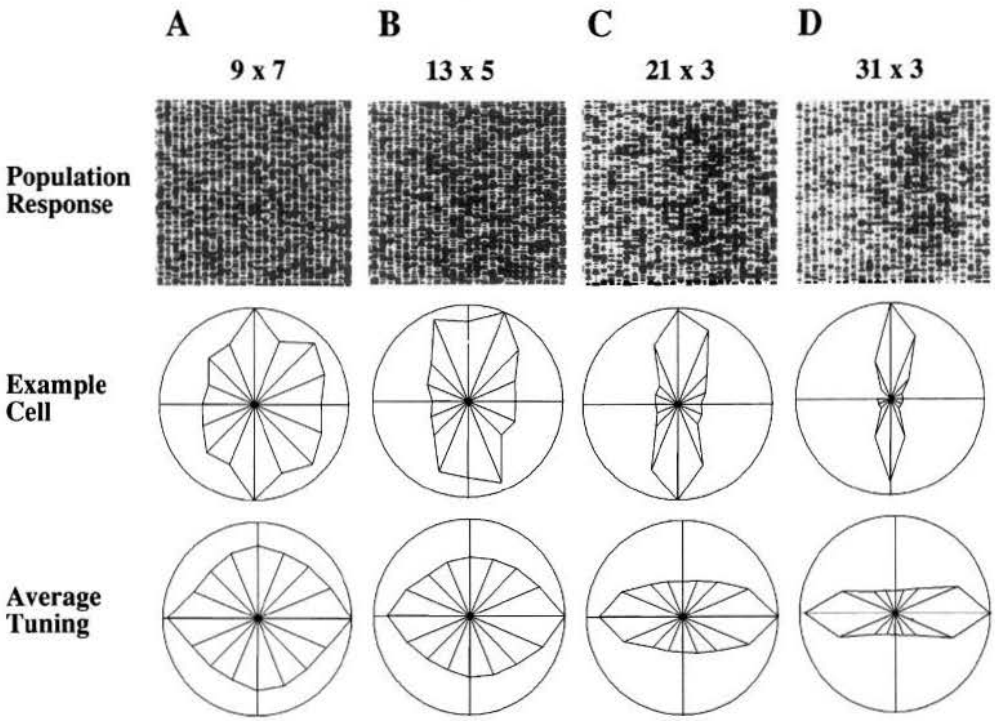

Figure 8. Orientation selectivity as a function of the aspect ratio in the absence of any corticocortical inhibitory connections. Different arrangements according to the HW model are characterized by the number of geniculate cells converging onto each cortical cell (e.g., nine rows by seven columns of geniculate cells). This amounts to receptive field width:length ratios of 1.16, 1.78, 3.18, and 4.40 for the 9 × 7, 13 × 5, 21 × 3, and 31 × 3 receptive field arrangements, respectively, and leads to the average orientation tuning indicated in the *bottom row.* The average tuning of inhibition was obtained from 55 cells randomly selected and rotated to a common preferred direction prior to averaging. The *middle row* illustrates the response of one "typical" cell. The same cell will also be shown in the *middle row* of the following figures. The *top row* shows the cumulative spike count across one orientation column, accumulated during a 1000-msec-long stimulation with a moving vertical bar. Cells with an approximately horizontal preferred orientation are represented on the *left side* of each panel, whereas cells with vertical preferred orientation are clustered on the *right side.*

1982). This connection scheme assumes that only cells with an orientation that is approximately orthogonal to the center cell contribute to inhibition. Because our simulation models the cortical columns as vertical stripes, these cells are found at the distance of half a hypercolumn to the left and to the right of the cell in the center (Fig. 9*D*). Partial circular inhibition (Fig. 9*C*) uses the same annulus of cells as candidates for connections, but the a priori probability drops to 0 as soon as the angle as shown in Figure 9 is larger than 45°. Consequently, only about 50 cells connect to each target cell.

In *local* inhibition, neighboring cells with similar orientation tuning but laterally displaced receptive fields project onto the center cell (Heggelund, 1981; Koch, 1987). Thus, in the relatively unspecific "local" scheme (Fig. 9*D*), the a priori probability of a connection is high between 100 and 300 μm away from the central cell, being very small for smaller and larger distances. In addition, the a priori probability is lowered along the long axis of the receptive field of the target cell, to provide the necessary asymmetry in the inhibition. About 30 cells converge onto each central cell in this connection procedure. In the local scheme (Fig. 9*D*), an overlap between inhibitory receptive fields similar to that shown in the right part of Figure 9*E* occurs, but arising from many more cells and also much more unspecific than for the *sparse local* inhibition wiring. Sparse local connections (Fig. 9*E*) are defined by only two cells that inhibit the center cell. The two cells were selected in a highly specific manner as those cells whose receptive fields maximally overlap the field of the center cell. We explored the functional consequences of this wiring scheme in order to understand the limiting case of a very specific inhibitory wiring.

Figure 10 shows simulated activity functions for one cell demonstrating how the different inhibitory connection schemes influence the shape of the receptive field. Connections to the cell were determined by the simulator; gain values for the connections were set to the average gain for each connection scheme multiplied by a normalization factor to achieve similar peak heights. Figure 10, *A* and *B,* represents a cortical receptive field generated by a convergence of 5 × 13 LGN receptive fields viewed edge-on from two different angles. As expected, the receptive field elongation is about 1.7. Inhibitory cells contribute to the receptive field shape of the target cell in all other panels. The remaining panels illustrate the effect of superimposing the various inhibitory schemes onto the basic HW connectivity (negative regions denote inhibition). Random inhibition (Fig. 10*C,D*) influences the receptive field elongation least of all and leads to a more or less isotropic "bowl" of inhibition around the center peak. Circular inhibition (Fig. 10*E,F*) and partial circular inhibition (Fig. 10*G,H*) act very similarly on this particular cell, increasing the elongation of the receptive field significantly. The "bowl" of inhibition disappears, and more realistic side bands can be observed. Local inhibition (Fig. 10*I,J*) has the strongest effect on the receptive field elongation because the inhibitory cells are located close to the target cell. This, however, also reduces the length (Fig. 10*J*) of the receptive field substantially. The side bands are pronounced, but there is also some inhibition along the long axis of the receptive field (Fig. 10*I*). This effect arises due to the low specificity of the local connection scheme and disappears for sparse local inhibition (Fig. 10*K,L*). The influence of the two inhibitory cells is clearly discernable, and true sideband inhibition can be observed. Apparently the "right" inhibitory receptive field (Fig. 10*K*) is closer to the center of the peak than the "left" field.

Unless otherwise mentioned, the gain values for the LGN-to-cortex connections were held at the same level during the simulations shown in the remaining figures. The gains of the inhibitory connections were adjusted to obtain similar overall activity levels. The same "example" cell as in Figure 8 is shown in Figures 11–15.

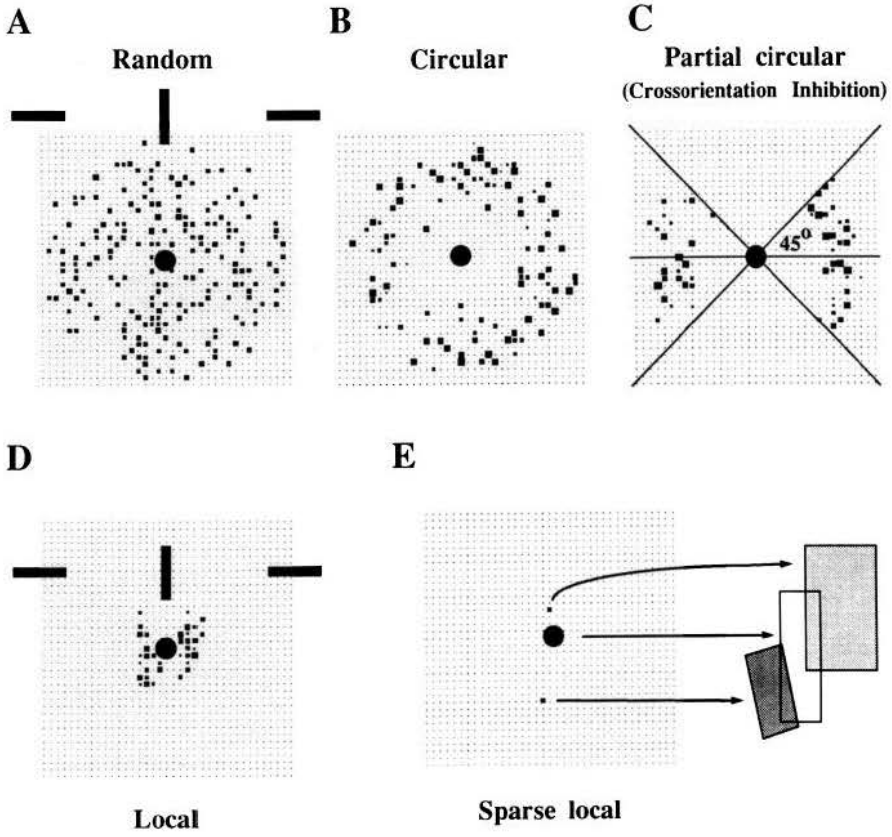

Figure 9. Different intracortical inhibitory connection schemes. The central cell (*large spot*) receives inhibitory input from cells indicated by the *small squares*. The size of these squares encodes the axonal delay. Because the delays for local connections are much smaller than those for long-distance connections, their size has been exaggerated graphically. A sketch of the column structure as determined by the afferent LGN connections is superimposed in *A* and *D* (*solid bars*).

The central topic of this study is to compare the specificity of various intracortical connection schemes. Let us therefore define what we mean by "specificity." The specificity of a connection scheme is related to the number of parameters that specify whether a connection between two given cells is established. For instance, only the radius of the disk has to be specified for random inhibition, whereas circular inhibition requires already two parameters (the outer and the inner radius of the annulus), and partial circular inhibition, yet another parameter: the angle within which connections are made. Thus, the level of "specificity" in these connection schemes increases from random to partial circular inhibition (and similarly from local to

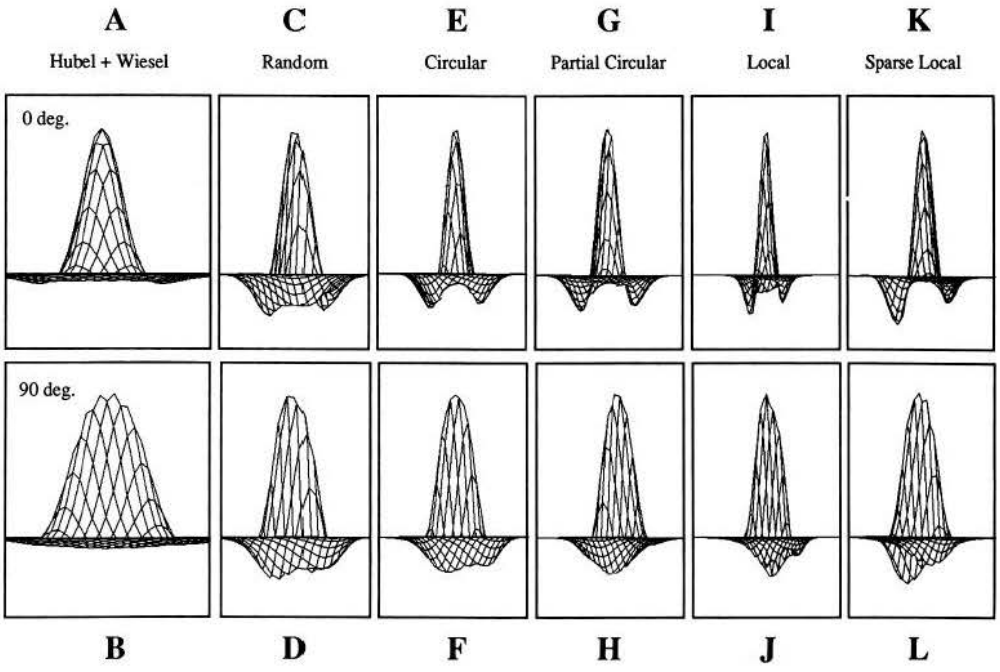

Figure 10. Effects of the different inhibitory connection schemes on the spatial shape of the receptive field of one example cell. Diagrams show receptive field activity functions computed from a superposition of basic receptive field types viewed edge on. *A* and *B*, A superposition of DOGs (see Eq. 6) determines the HW-type receptive field of the target cell. *C–K*, The HW fields of the inhibitory cells are determined in a similar manner and are then subtracted from the excitatory receptive fields for the different inhibitory connection schemes.

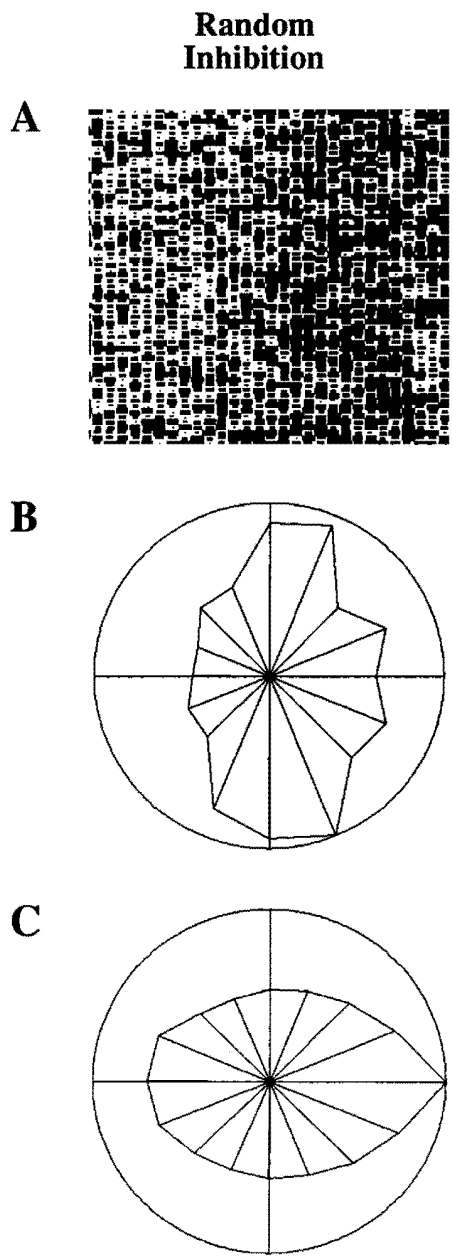

Figure 11. Orientation selectivity achieved with HW-type connections (aspect ratio, 13 × 5) and additional random inhibition (see Fig. 9*A*). *A*, Cumulative spike count across one orientation column (1000-msec sweep, vertical-bar stimulus). *B*, Example cell. *C*, Average orientation tuning.

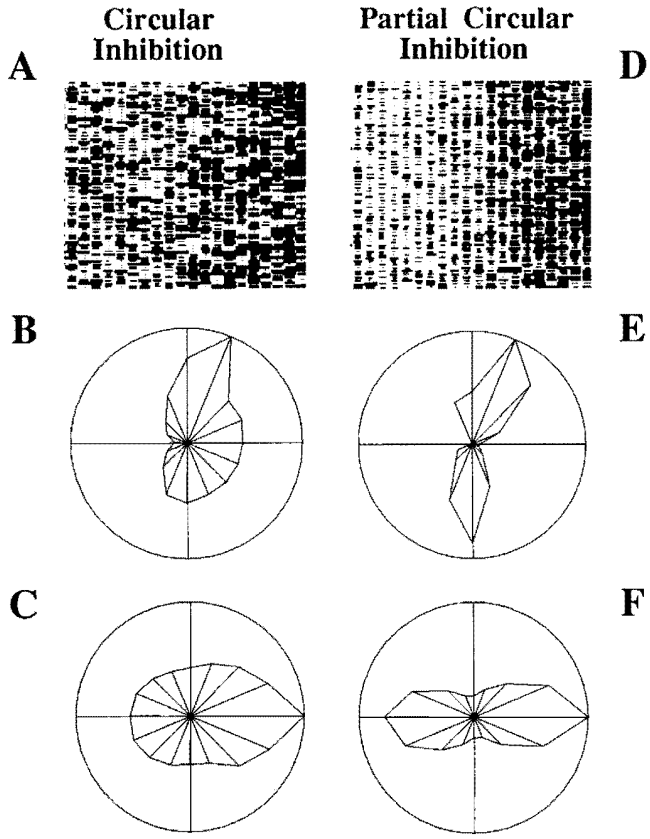

Figure 12. Orientation selectivity achieved with HW-type connections (aspect ratio, 13 × 5) and additional circular (*A–C*) or partial circular (*D–F*) inhibition (see Fig. 9*B,C*). *A* and *D*, Cumulative spike count across one orientation column (1000-msec sweep, vertical-bar stimulus). *B* and *E*, Example cell. *C* and *F*, Average orientation tuning. Note the significant average directional bias generated with circular inhibition (*C*).

sparse local). In the following, we will always use "specificity" in this sense of minimal description length.

Unspecific random inhibition

In comparing the specificity of the different schemes, *random* inhibition serves as a control to illustrate the sharpening of orientation tuning that can be achieved without very specific inhibitory connections (Bonds, 1989). This can be seen most easily when one considers the value of the $\theta_{1/2}$ parameter of the orientation tuning curve. The more activity is subtracted from this curve, the more the tuning curve will be clipped (an effect called "iceberging") and $\theta_{1/2}$ will change. Thus, the effect of unspecific inhibition onto the orientation tuning depends in a nonlinear way on the basic activity level that the cells show without inhibition. Random inhibition sharpens the orientation tuning more efficiently at lower basic activity levels. However, because we are primarily interested in the differences of specificity that can be achieved by different connection schemes, we operate our simulation in the linear range. Thus, we use reasonably large values of activity arising from the HW-type connections. Therefore, on average, only a weak effect of sharpening the orientation tuning with random inhibition is seen in Figure 11*C* [$O = 20.7\%$ (54.9°) as compared to 18.6% (57.8°) in Fig. 8*B*]. The orientation columns (Fig. 11*A*) remain about as fuzzy as for the mere HW-type connections, and the example cell even shows a loss of orientation tuning [$O = 26.6\%$ (48.0°)] as compared to Figure 8*B* [$O = 37.3\%$ (38.7°)]. However, with random inhibition, a slight directional bias arises [Fig. 11*C*; $D = 12.6\%$ (28.3%)]. This effect was relatively robust against variations of gain parameters and also occurred with other inhibitory connection schemes (see Figs. 12–15).

Circular and partial circular inhibition

Circular inhibition increases the orientation tuning more than does random inhibition; however, the resulting average tuning strength [Fig. 12*C*; $O = 32.2\%$ (42.7°)] is still much weaker than the one found in real simple cells. Circular inhibition results in a rather strong directional bias with an average D component

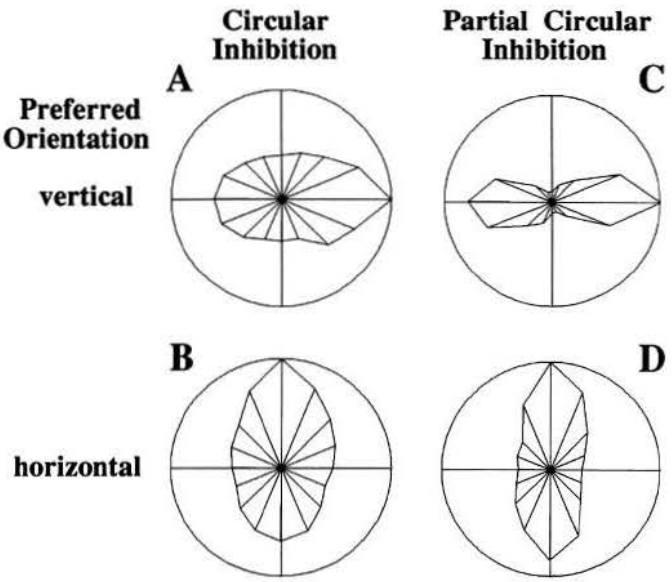

Figure 13. Differences in the average orientation tuning for cells with vertical (*A, C*) and horizontal (*B, D*) preferred orientations obtained by circular and partial circular inhibition added onto HW-type receptive fields (aspect ratio, 13 × 5). The average orientation tuning is similar for both populations implementing circular inhibition (*A, B*) and significantly different using partial circular inhibition (*C, D*).

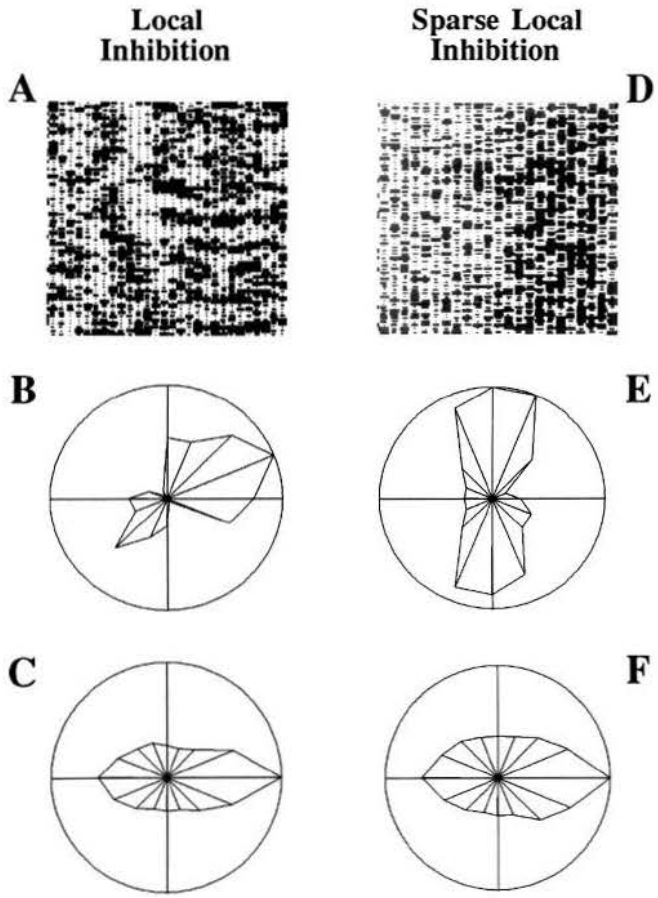

Figure 14. Orientation selectivity achieved with HW-type connections (aspect ratio, 13 × 5) and additional local (*A–C*) or sparse local (*D–F*) inhibition (see Fig. 9*D,E*). *A* and *D*, Cumulative spike count across one orientation column (1000-msec sweep, vertical-bar stimulus). Note that local inhibition destroys the columnar structure. *B* and *E*, Example cell. *C* and *F*, Average orientation tuning.

of 23.0% (44.2%), twice as much as for random inhibition. This result is intriguing, because circular inhibition seems to be entirely isotropic. Any inhibitory influence that arises along a particular direction of stimulus motion should be, on average, identical to that from the opposite direction. Although the cells for averaging have been selected from the central part of the simulated patch, a possible asymmetry between the responses in two opposite directions could arise from border effects in the simulation. To rule out this artifact, we separated the 55 cells according to their location and relative to their preferred direction of motion. The actual preferred direction was then compared with the preferred direction that would be predicted by the border-effect artifact. Thus, border effects do not contribute significantly to the directional bias. The actual reason for the generation of a directional bias is a hidden anisotropy (see Intracortical inhibitory mechanisms, in Discussion).

Partial circular inhibition (Figs. 8*B*, 12*D–F*) has a more powerful effect on orientation tuning. This connection scheme is more specific than circular inhibition, because it assumes that only cells on the annulus within a given angle (45°) will be connected to the center cell. Because those cells have a preferred orientation approximately orthogonal to that of the center cell, partial circular inhibition is closely related to cross-orientation inhibition.The column structure is significantly sharpened (Fig. 12*D*). The average tuning is about as strong [Fig. 12*F*; O = 73.7% (20.1°)] as those found in real cells, and the directional bias is reduced [D = 10.2% (22.7%)].

Another intriguing finding resulting from long-range inhibition is shown in Figure 13. Cells with a vertical and a horizontal preferred orientation exhibit different average tuning strengths when using partial circular (i.e., cross-orientation) inhibition [Fig. 13*C,D*; O = 96.0% (12.8°) vs. O = 55.2% (28.0°)]. This difference disappears for circular inhibition [Fig. 13*A,B*; O = 33.9% (41.3°) vs. O = 29.6% (45.0°)]. The difference between partial and circular inhibition can be explained by an anisotropy that involves the arrangement of inhibitory cells and their target cell relative to the stimulus orientation. When using a flashing elongated bar stimulus, a cell with vertical preferred orientation receives its cross-orientation inhibition from cells with horizontal preferred orientations half a hypercolumn away. A horizontally oriented bar stimulus will cover the receptive fields of these cells optimally and thus induce strong inhibition. In turn, horizontal-oriented cells receive cross-orientation inhibition from their orthogonal counterparts at the same distance. In our artificial vertical-stripe column system, a vertical-bar stimulus, however, will basically stimulate only cells within the same column. Thus, in this case no cross-orientation inhibition is induced, and consequently, orientation tuning is not sharpened. This simplified argument excludes the existing receptive field overlap and does not elaborate on possible effects caused by the artificial (stripelike) column structure. These questions are addressed elsewhere (Wörgötter et al., 1991b). Suffice it to say that this study provides evidence that the unwanted inherent anisotropic behavior of cross-orientation inhibition can also persist in a real cortex. We feel that this makes it unlikely that this particular cross-orientation inhibition scheme exists in real cortex. This is the principal reason for us to consider a modified cross-orientation scheme, circular inhibition.

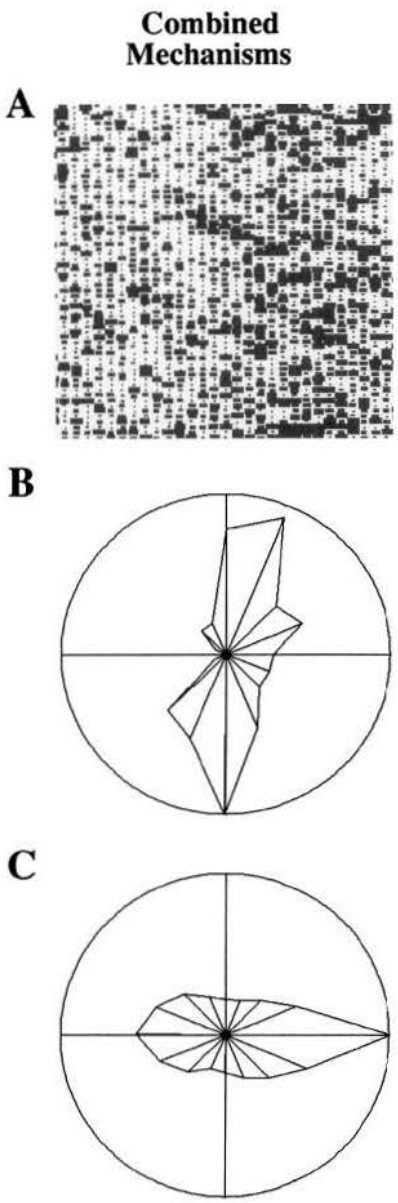

Figure 15. Orientation selectivity achieved with HW-type connections (aspect ratio, 13 × 5) and additional local as well as circular inhibition. *A,* Cumulative spike count across one orientation column (1000-msec sweep, vertical-bar stimulus). *B,* Example cell. *C,* Average orientation tuning.

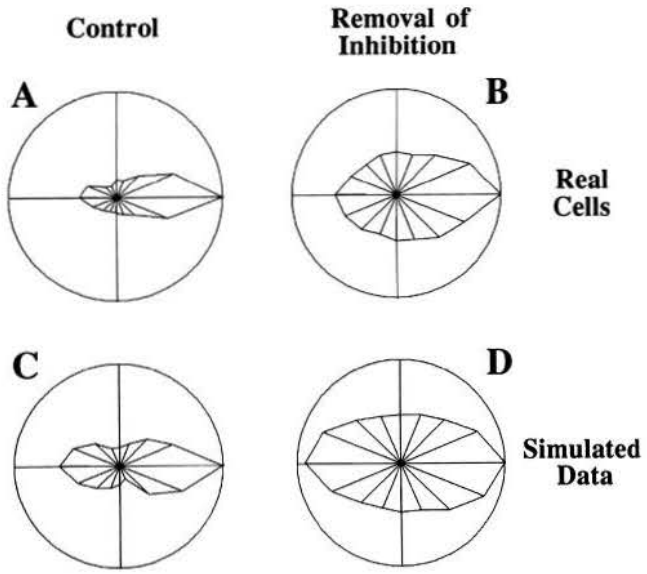

Figure 16. Comparison of the average orientation tuning of real cortical simple cells with that obtained from the model. *A,* Average orientation tuning of observed cortical simple cells. *B,* Average orientation tuning of cortical simple cells after removal of intracortical inhibition during microiontophoretical application of GABA lateral to the recorded cell (Wörgötter and Eysel, unpublished observations). *C,* Average orientation tuning of simulated cells achieved with HW-type connections (aspect ratio, 13 × 5) and additional local as well as circular inhibition. (Gain parameters were chosen differently from those used in Fig. 15.) *D,* Average orientation tuning of simulated cells after reducing the gain of intracortical inhibition to 10% of their original value. Note the similarity of the orientation tuning between *A* and *C* and between *B* and *D*. The average directional tuning of real cells, however, is larger than that of the simulated cells.

Local inhibition

Local inhibition can be implemented in less specific ("local," Fig. 9*D*) or in a more specific manner ("sparse local," Fig. 9*E*). Both mechanisms strengthen the orientation tuning substantially (Fig. 14*B,C,E,F*), and average values of $O = 48.7\%$ (31.4°) are reached with local and $O = 39.7\%$ (37.0°) with sparse local inhibition. With sparse local inhibition, the column structure is enhanced (Fig. 14*D*), whereas the unspecific local inhibition destroys the columnar structure (Fig. 14*A*), even though orientation tuning is stronger (Fig. 14*B,C*). The loss of orientation columns is due to the fact that many cells that originally belonged to a horizontal column change their behavior and now respond best to vertical stimuli (Fig. 14*B*). The effect of strengthening the orientation tuning with the unspecific local connection scheme is very robust against variations in the parameters that determined the actual connections.

The strongest enhancement of orientation tuning with sparse local inhibition was found when the distance between the receptive field of the source and the target cell was larger than 0.15°, because otherwise, inhibition will affect all orientations of the target cell in a similar manner.

Both connection schemes result in a rather strong directional bias [Fig. 14*C,F*; $D = 18.7\%$ (38.8%) and 15.3% (33.4%), respectively]. Only a few (for sparse local, only two) cells contribute inhibition to the center cell. Thus, any random asymmetry between the total inhibition that arises for an optimally oriented stimulus along both directions of motion will result in a net difference between the responses and, thus, in a directional asymmetry.

Combining local and circular inhibition

The low-specificity mechanisms (local and circular inhibition) alone are not sufficient to generate realistic orientation tuning. Combining both with different gains (which distinguishes this combination from random inhibition), however, resulted in a reasonable strength for the orientation specificity (Figs. 15, 16*C*). The column structure is clearly visible (Fig. 15*A*), but, as in the real cortex, a significant number of cells are found that respond to stimuli orthogonally oriented to their expected preferred orientation. The directional bias is substantial [Fig. 15*C,D*; $D = 22.2\%$ (43.3%) and 25.0% (46.4%), respectively], but still much weaker than the average observed directional tuning of simple

cells [Fig. 16*A*;*D* = 57.2% (68.3%)]. Otherwise, the averaged simulated tuning curve [Fig. 16*C*; *O* = 69.6% (21.6°)] looks very similar to the average observed cortical tuning [Fig. 16*A*; *O* = 73.5% (20.1°)].

Recently, Wörgötter and Eysel (unpublished observations) reported that the orientation tuning of cortical cells can be strongly influenced by microiontophoretic application of GABA to the upper cortical layers at a lateral distance of about 0.5 mm (see also Sillito, 1975; Sillito et al., 1980). The most common effect found was a loss of orientation specificity due to increased responses in the nonpreferred orientations. This resulted in an average orientation tuning of *O* = 34.6% (40.8°), as shown in Figure 16*B*. Reduced orientation tuning due to increased responsiveness was interpreted as a loss of inhibition, caused by inactivation (via the GABA application) of intracortical inhibitory interneurons. We simulated GABA application by removing most intracortical inhibition for the last simulation. In the run shown in Figure 16*D*, the gain of the inhibitory intracortical mechanisms was reduced to about 10% of their original values. The simulated orientation tuning [*O* = 39.6% (37.1°)] is remarkably similar to the observed tuning curve upon GABA application (Fig. 16*B*), though it is still stronger than with mere HW-type connections (Fig. 8*B*).

Discussion

Assumptions

This numerical study examines the question of the wiring scheme underlying orientation selectivity in the input layer of primary visual cortex of the adult cat. With one exception (see below), we did not study the network properties underlying other operations, such as direction selectivity or stereo disparity. Furthermore, we have made no attempt to study the developmental origin of the various inhibitory connection schemes. We briefly consider below the question of which connection scheme is more likely to arise during development without postulating highly specific mechanisms.

Our computer model was primarily constrained by two factors, the lack of sufficient anatomical and electrophysiological data and the long simulation times. Let us here briefly restate our main assumptions and their limitations.

Underlying our network simulation is a model of a single neuron representing an elaboration of the much simpler "leaky integrate-and-fire" model, but stopping short of a full Hodgkin and Huxley (1952) type of description. It shows all of the basic properties characterizing neurons: electrotonic response, threshold, absolute and relative refractory period, nonlinear interaction among synaptic conductance inputs, and finite axonal propagation velocity. Its principal drawback is the assumption of a one-compartment neuron. Thus, local nonlinear interaction among synaptic inputs in the dendrite of cortical cells (Koch and Poggio, 1987) or local membrane nonlinearities in the dendrites are not incorporated into our current model. However, we have seen no evidence to date implying the necessity of such nonlinear interactions to explain orientation selectivity. We do believe, however, that a more complete network model, incorporating the selectivity of individual cortical cells to orientation, motion, color, depth, texture, and so on, requires cells with many compartments to support local, nonlinear operations prior to the somatic nonlinearity (Koch and Poggio, 1987).

Our model of the early visual pathway of the adult cat is quite realistic with regard to cell numbers, degree of anatomical divergence and convergence, and basic receptive field properties. We studied in great detail the contribution made by local and long-range inhibitory wiring schemes to orientation selectivity. There is evidence for the existence of long-range inhibition (Martin et al., 1983; Gilbert, 1985), and its role in the generation of orientation selectivity has been discussed (e.g., Benevento et al., 1972; Sillito, 1979; Bonds, 1989; see also Martin, 1988). We restricted ourselves to investigating the effects of different long-range schemes on orientation tuning instead of other possibilities (e.g., contrast gain control; but see Wehmeier et al., 1989). We completely disregarded in this study excitatory corticocortical connections as explicitly modeled by Douglas et al. (1989). We first wanted to understand the contributions made by the negative feedback pathways before attempting to assess the contribution made by positive feedback circuits. Excitatory cortical connections can lead to a very rich dynamic behavior, including oscillations, chaos, and epileptic seizures (Wilson and Cowan, 1972; Hopfield, 1984; Kammen et al., 1989). Because of this restriction, we need not explicitly model excitatory cortical cells, such as pyramidal cells, because in the absence of such excitatory corticocortical connections, the receptive fields of excitatory pyramidal cells will be identical to that of inhibitory cortical cells. This assumes that a given pyramidal cell receives the same pattern of inhibition as inhibitory cells. In the next phase of our project, we will include a large population of excitatory pyramidal cells, providing excitatory feedback.

Finally, we wish to point out that this article represents but an interim report in our multiyear effort to understand information processing in realistic cortical structures.

The Hubel and Wiesel model

As shown by Figures 5–7, many basic features can be mimicked by an HW-type afferent arrangement. These include null response (Movshon et al., 1978) and velocity as well as orientation tuning. However, several features are not explained in a satisfactory manner by the HW scheme.

In order to achieve nonoverlapping ON–OFF-subfields without intracortical inhibition, the spatial separation of the projections from LGN to cortex had to be rather large (Fig. 5*E,F*). In fact, we only found realistic separation between ON- and OFF-subfields with a spacing of 0.5° or larger between the center of LGN cells. Sillito (1975) stated that application of bicuculline resulted in a loss of the ON–OFF-subdivision in simple cells. In addition, experiments (Wörgötter and Eysel, unpublished observations) involving removal of intracortical inhibition led to a substantial widening of the subfields, interpreted as a loss of side-band inhibition. This supports the view that cortical subfields are highly overlapping and that this overlap is reduced or eliminated by intracortical inhibition.

Without cortical inhibition, our simple cells have an approximatively constant response if the velocity of a moving bar is varied between 0.1 and 5°/sec. Velocities higher than 5–10°/sec lead to a monotonic decreasing cellular response (Fig. 5*D*). Such "velocity low-pass" behavior is typical for about 60% of simple cells in cat area 17 (Orban et al., 1981). Band-pass, that is, "velocity-tuned," behavior (Orban et al., 1981) was only found in 12% of the cells following the introduction of intracortical inhibition. Such behavior is the natural consequence of a low-pass–velocity cell inhibiting other low-pass cells (subtracting two low-pass filters leads to a band-pass filter).

The HW model also reproduces the response of cortical cells to moving spots (Fig. 7), a response that is stronger parallel to the long axis of the receptive field than orthogonal to this axis

(Wörgötter and Eysel, 1989). Hence, the preferred axis of motion for a spot is orthogonal to that of a bar. This phenomena is caused by subsequent stimulation of two sites within the receptive field of a cell, resulting in a larger response than the sum of the two individually elicited responses. This effect is due to the temporal integration that occurs at all stages in the model (Henry et al., 1978; Wörgötter and Holt, 1991). Thus, if a spot travels exactly along the long axis of the receptive field, the longest possible path for such a stimulus to stay within the receptive field, this temporal summation will lead to a stronger response than motion orthogonal to the long axis.

As evident in Figure 8, the orientation tuning of simple cells is directly related to the aspect ratio of their associated geniculate input, that is, to the length : width ratio of the receptive field. The only study to have correlated aspect ratio to $\theta_{1/2}$ in cat simple cells (Watkins and Berkley, 1974) found a relatively small correlation coefficient of $r = 0.47$ between these two variables. For instance, many cells with very small aspect ratios still possess reasonable orientation tuning, because they consist of multiple subfields, each of which has a much higher aspect ratio (Daugman, 1980, 1984; Jones and Palmer, 1987). In fact, in order to account for the average orientation tuning in cat area 17 simple cells (with $\theta_{1/2}$ less than 20°; Orban, 1984), the ratio of length to width has to be 4.0 or higher. While there undoubtedly exist cells with such aspect ratios, they are rare in the input layer but are much more frequent in layer 5 and, in particular, layer 6 (Gilbert, 1977). Thus, although in principle the HW model can by itself account for the strong orientation tuning observed, the small number of cells with large receptive field elongation indicates that additional mechanisms must be involved.

A further reason for arguing against a pure HW model is its lack of gain control. If the contrast of the bar stimulus is decreased, geniculate cells will fire less. Ultimately, there will be a point at which cortical cells will fail to respond, because not enough geniculate-induced EPSPs are present to exceed the voltage threshold. If, however, cortical inhibition is superimposed onto the HW scheme, as in this study, a reduced geniculate input will cause less EPSPs but also less IPSPs. Thus, the response to cortical cells should be far less dependent on contrast in the mixed models than in the pure HW threshold model. In other words, models relying on negative feedback have inherent gain-control properties not shared with feedforward threshold-type models. This has been demonstrated in our earlier simulations (see Wehmeier et al., 1989, their Figs. 10.7 and 10.8). It has been shown experimentally using cats adapted to varying levels of contrast that the orientation tuning of area 17 simple cells changes little when varying the contrast between 2% and 80% (Skottun et al., 1987). However, in order to rule out long-term adaptation of cortex due to shifts in firing threshold caused by second-messenger–mediated responses, these experiments should be repeated by randomly intermixing bars of low and high contrast in the stimulus sequence.

An alternative candidate mechanism is based on orientation-sensitive geniculate input. It has been reported (Vidyasagar and Urbas, 1982; Cleland et al., 1983; Schall et al., 1986; Vidyasagar, 1987; Shou and Leventhal, 1989) that geniculate cells are not circularly symmetric, but do show significant asymmetries for the orientation of bars and gratings. This orientation sensitivity is particularly pronounced at spatial frequencies above 1 cycle per degree. While we have assumed rotational invariant LGN receptive fields in our model, oriented geniculate cells would be difficult to distinguish from an HW type of arrangement. Of course, both mechanisms could well contribute toward cortical orientation selectivity.

The multitude of effects that can be explained using an afferent bias in orientation strengthens the view that the fundamental cortical response characteristic is, in fact, generated by such a connection scheme. For this reason, we are interested in the question of what cortical wiring scheme has to be superimposed to better mimic experimentally observed behavior.

Intracortical inhibitory mechanisms

Intracortical inhibition was superimposed onto HW connections with the very low aspect ratio of 13 × 5. We did not investigate the effect of the inhibitory mechanisms in the absence of afferent orientation bias, because all but the sparse local mechanism require at least a small bias to initiate further sharpening of the orientation tuning [Sillito (1979) discussed this problem for cross-orientation inhibition]. As expected, orientation tuning was strengthened substantially with any highly specific inhibitory mechanism. Mechanisms with low specificity contributed less to the sharpening of orientation tuning but were much more robust against parameter variations. With the unspecific local inhibition scheme, the predetermined orientation columns were destroyed (e.g., Fig. 14*A*). Due to the receptive field scatter and the variations of the predetermined preferred orientations within one column, the cortical topography is not preserved below distances of about 200 μm (Albus, 1975a). Thus, any local inhibition scheme that relies entirely on neighborhood relationships between cells will not be able to preserve the column structure. Circular inhibition acts over a radius of about 500 μm, within which the cortical topography is well defined. Combining circular with local inhibition enhanced orientation columns and generated a realistic orientation tuning (Fig. 15). Most experimental results about local and cross-orientation inhibition showed that the orientation tuning of the inhibition itself is rather broad (Blakemore and Tobin, 1972; Albus and Baumfalk, 1989; Bonds, 1989; Wörgötter and Eysel, unpublished observations; but see Hata et al., 1988). This is in agreement with our simulations with the combined low-specificity mechanisms. The existence of long- as well as short-range inhibitory mechanisms in real cortex can also account for seemingly conflicting experimental results that provide evidence for one or the other mechanism. Biases towards either mechanism can in many cases be explained by the fact that the experimental methods cannot show both long- and short-range mechanisms simultaneously. A key advantage of such a combination is its inherent robustness against structural and parameter changes. From the developmental point of view, low-specificity inhibitory mechanisms are easier to create because they require only little structural information, for example, about dendritic tree radii, axonal arborization, axonal and dendritic tree orientation and elongation, and so on. The low-specificity mechanisms implemented in the model, however, might only reflect an early developmental stage because during the maturation process higher specificity can be achieved by eliminating inhibitory connections (Beaulieu and Colonnier, 1987). Thus, the more specific connection schemes (sparse local and partial circular) could be derived from the low-specificity mechanisms by pruning inefficient connections.

We have excluded the OFF-subsystem while simulating the effects of intracortical inhibition. We are well aware that this is a serious omission. However, including the ON–OFF-subsystem as well as intracortical inhibition increases the computa-

tional time to more than 150 hr of CPU time on our SUN-4 workstations for simulating a 1-sec experiment, making it impractical to explore this wiring scheme. We could therefore not investigate the so-called "push–pull" class of models (Hubel and Wiesel, 1962; Ferster, 1988; Tolhurst and Dean, 1990), in which activity in ON-subfields will inhibit activity in spatially overlapping OFF-subfields (mediated via inhibitory cortical interneurons) and vice versa (see also Toyama et al., 1981). We have now started to run our simulator on the 16,000-processor Connection Machine, a machine powerful enough to make such simulations feasible.

Cross-orientation inhibition (i.e., partial circular inhibition; Benevento et al., 1972; Morrone et al., 1982) resulted in different average orientation tuning for the populations with vertical and horizontal axes of preferred orientation. This effect is explained by the arrangement of the cells that contribute inhibition relative to the orientation of the stimulus (see Results; Wörgötter et al., 1991b). The sharpening of orientation tuning by cross-orientation inhibition is substantial. This is in disagreement with recent studies on the effect of long-range inhibition finding a rather broad tuning (Bonds, 1989; Wörgötter and Eysel, unpublished observations). A new type of long-range lateral inhibition, which we call "circular inhibition," does not lead to different tuning for different cell populations. In combination with local inhibition, it yields tuning curves very similar to experimentally observed ones (e.g., Figs. 15, 16) and does not destroy the columnar substructure as local inhibition does by itself (Fig. 14*A*). Circular inhibition will always produce a certain amount of end-stopping, which, however, is very common in layer IV of the cat (Gilbert, 1977).

Thus, we propose that the average orientation selectivity of simple cells is mediated by at least three different connections: a weak afferent geniculate bias (Hubel and Wiesel, 1962; Vidyasagar and Urbas, 1982) superimposed onto local inhibition, functionally acting as iso-orientation inhibition, and onto circular inhibition, corresponding to a very broadly tuned cross-orientation inhibition. In other words, we argue for an eclectic model of orientation selectivity.

Recent intracellular recordings (Sato et al., 1990) do find these two inhibitory components: a strong iso-orientation inhibitory component and a broadly tuned inhibition acting primarily at nonpreferred orientations. Furthermore, our conclusion is also in agreement with that of Bonds (1989), who used two superimposed sine-wave gratings to study this question.

It should be emphasized at this point that, due to random variations in the connection pattern and synaptic strength (see Structure of the Model), the behavior of individual neurons varies quite a bit. Thus, in some cells the afferent geniculate bias is quite strong, and inhibition only contributes insubstantially toward orientation tuning, while for other cells little tuning is present in the absence of intracortical inhibition. Therefore, we propose that, to explain the average orientation tuning of layer VI simple cells, three different mechanisms are required, while some cells may only possess one or two of these mechanisms.

Excitatory and inhibitory connections differ not only with respect to their action at the postsynaptic target but presumably also in the way they develop in the immature animal. Coactivation of the pre- and postsynaptic cells can result in the strengthening of an excitatory connection (Hebb, 1949). Such a Hebbian mechanism presumably plays a major role in the development of excitatory connections (Miller et al., 1989). Inhibitory connections cannot be strengthened by the same mechanism, because activation of the presynaptic cell will silence instead of coactivate its postsynaptic target. Thus, the strengthening of inhibitory interactions is more difficult to achieve during development. It is interesting to note that experimental efforts to uncover modifications of inhibitory circuits in visual cortex have consistently yielded negative results (Singer, 1977; Bear et al., 1985). Circular inhibition requires little specificity, because it only assumes that cells within a given distance inhibit the center cell. Thus, no Hebb-type enhancement of connections is required.

Spontaneous generation of direction selectivity

The most intriguing result of the simulation was the "spontaneous" generation of directional bias. Thus, a rule that only specifies "make inhibitory synapses onto cells about 500 μm away" leads to the amplification of preexisting orientation selectivity as well as to the *de novo* generation of a directional bias, a bias not present in the geniculate input.

Even though an isotropic connection scheme represents the "worst" case for the generation of an anisotropic effect, the generation of a directional bias is not directly linked to circular inhibition and occurs to some extent in all of our inhibitory connection schemes (Figs. 11–15). Any single pair of connections of arbitrary length will cause directional tuning because the source cells are likely to have different response characteristics due to the noise in the column structure (noise-induced symmetry breaking). This can be clearly seen in the case of sparse local inhibition (e.g., Fig. 14*F*). However, if the preferred orientations were arranged randomly in cortex, this effect would average out with increasing number of connections onto a given cell. But why does this not occur with circular inhibition, where more than 100 cells converge onto a target? Two structural features inherent in cortical columns underlie our effect: (1) cell activities are locally correlated, but (2) the correlation disappears over long distances. It is obvious that long-range connections that terminate in a locally confined region of such a structure will induce an anisotropic effect that will not necessarily average out with increasing number of connections. We show elsewhere that this directional bias does not depend on the specific geometry of the columnar structure adopted (e.g., straight vs. bent columns; Wörgötter et al., 1991b). Furthermore, jitter in the anatomical layout and in biophysical parameters only serves to enhance the orientation and directional tuning obtained with circular inhibition. Thus, it would be difficult not to achieve a directional bias when considering inhibitory (or excitatory, because this effect does not depend on the sign of the interaction) intracortical connections.

The directional bias seldom exceeded values of 20%, much lower than the averaged observed directional tuning of simple cells (D = 60%; see Orban, 1984). Such a bias, however, can represent the starting point in ontogenesis to strengthen connection patterns that increase direction selectivity as a useful feature in motion recognition tasks. This view is supported by several findings. Sillito (1975, 1977, 1979) observed that directional tuning of cells is more readily eliminated by microiontophoretical application than orientation tuning. Similarly, it has been found that removal of orientation tuning eliminates direction tuning entirely (Wörgötter and Eysel, unpublished observations), whereas direction tuning can be substantially reduced without affecting orientation specificity (Eysel et al., 1988). Furthermore, there are virtually no cells in area 17 that display

large direction specificity but only little orientation tuning (Wörgötter et al., 1991a). Finally, during the early stages of development, only a small number of cells are directionally selective, while most cells are only weakly biased. Their directional selectivity increases only after the development of orientation tuning (Grigonis et al., 1988). This would support our notion that directional tuning follows the emergence of orientation selectivity. We assume that, once this directional tuning is established, additional inhibitory (or excitatory) mechanisms sharpen this bias to lead to actual directional selectivity.

Finally, an interesting moral can be drawn from these detailed simulation studies. We initially did not expect any surprising results to emerge from our computer model, but were hoping for a more quantitative understanding of the mechanisms underlying orientation selectivity. Thus, we were all the more pleasantly surprised to be confronted with a number of phenomena that were not predicted a priori from the data, even though most of these phenomena can be explained a posteriori from simple qualitative models.

References

Albus K (1975a) A quantitative study of the projection area of the central and the paracentral visual field in area 17 of the cat. I. The precision of the topography. Exp Brain Res 24:159–179.

Albus K (1975b) A quantitative study of the projection area of the central and the paracentral visual field in area 17 of the cat. II. The spatial organization of the orientation domain. Exp Brain Res 24: 181–202.

Albus K, Baumfalk U (1989) Bicuculline induced changes in excitability and orientation selectivity of striate cortical neurons. Soc Neurosci Abstr 15:132.8.

Bear MF, Schmechel DE, Ebner FF (1985) Glutamic acid decarboxylase in the striate cortex of normal and monocularly deprived kittens. J Neurosci 5:1262–1275.

Beaulieu C, Colonnier M (1983) The number of neurons in the different laminae of the binocular and monocular regions of area 17 in the cat. J Comp Neurol 217:337–344.

Beaulieu C, Colonnier M (1987) Effect of the richness of the environment on the cat visual cortex. J Comp Neurol 266:478–494.

Benevento LA, Creutzfeldt OD, Kuhnt U (1972) Significance of intracortical inhibition in the visual cortex. Nature 238:124–126.

Bilge M, Bingle A, Seneviratne KN, Whitteridge D (1967) A map of the visual cortex in the cat. J Physiol (Lond) 191:116P–118P.

Bishop PO, Kozak W, Vakkur GJ (1962) Some quantitative aspects of the cat's eye: axis and plane of reference, visual field coordinates and optics. J Physiol (Lond) 163:466–502.

Bishop PO, Coombs JS, Henry GH (1973) Receptive fields of simple cells in the cat striate cortex. J Physiol (Lond) 231:31–60.

Blakemore C, Tobin EA (1972) Lateral inhibition between orientation detectors in the cat's visual cortex. Exp Brain Res 15:439–440.

Bloomfield SA, Hamos JE, Sherman SM (1987) Passive cable properties and morphological correlates of neurones in the lateral geniculate nucleus of the cat. J Physiol (Lond) 383:653–692.

Bonds AB (1989) Role of inhibition in the specification of orientation selectivity of cells in the cat striate cortex. Vis Neurosci 2:41–55.

Boycott BB, Wässle H (1974) The morphological types of ganglion cells of the domestic cat's retina. J Physiol (Lond) 240:307–410.

Braitenberg V, Braitenberg C (1979) Geometry of orientation columns in the visual cortex. Biol Cybern 33:179–186.

Cleland BG, Lee BB, Vidyasagar TR (1983) Response of neurons in the cat's lateral geniculate nucleus to moving bars of different length. J Neurosci 3:108–116.

Creutzfeldt OD, Kuhnt U, Benevento LA (1974) An intracellular analysis of visual cortical neurones to moving stimuli: responses in a cooperative neuronal network. Exp Brain Res 21:251–274.

Daugman JG (1980) Two-dimensional spectral analysis of cortical receptive field profiles. Vision Res 20:847–856.

Daugman JG (1984) Spatial visual channels in the Fourier plane. Vision Res 24:891–910.

Dawis S, Shapley R, Kaplan E, Tranchina D (1984) The receptive field organization of X-cells in the cat: spatiotemporal coupling and asymmetry. Vision Res 24:549–564.

Douglas RJ, Martin KAC, Whitteridge D (1988) Selective responses of visual cortical cells do not depend on shunting inhibition. Nature 332:642–644.

Douglas RJ, Martin KAC, Whitteridge D (1989) A canonical microcircuit for neocortex. Neural Computation 1:480–488.

Enroth-Cugell C, Robson JG (1966) The contrast sensitivity of retinal ganglion cells of the cat. J Physiol (Lond) 187:517–552.

Enroth-Cugell C, Robson JG, Schweizer-Tong DE, Watson AB (1983) Spatio-temporal interactions in cat retinal ganglion cells showing linear spatial summation. J Physiol (Lond) 341:279–307.

Eysel UT, Pape H-C, van Schayck R (1986) Excitatory and differential disinhibitory actions of acetylcholine in the lateral geniculate nucleus of the cat. J Physiol (Lond) 370:233–254.

Eysel UT, Pape H-C, van Schayck R (1987) Contributions of different inhibitory mechanisms to the shift responses of X and Y cells in the cat lateral geniculate nucleus. J Physiol (Lond) 388:199–212.

Eysel UT, Muche T, Wörgötter F (1988) Lateral interaction at direction selective striate neurones in the cat demonstrated by local cortical inactivation. J Physiol (Lond) 399:657–675.

Ferster D (1986) Orientation selectivity of synaptic potentials in neurons of cat primary visual cortex. J Neurosci 6:1284–1301.

Ferster D (1987) Origin of orientation-selective EPSPs in simple cells of cat visual cortex. J Neurosci 7:1780–1791.

Ferster D (1988) Spatially opponent excitation and inhibition in simple cells of the cat visual cortex. J Neurosci 8:1172–1180.

Ferster D, Koch C (1987) Neuronal connections underlying orientation selectivity in cat visual cortex. Trends Neurosci 10:487–492.

Ferster D, Lindström S (1983) An intracellular analysis of geniculocortical connectivity in area 17 of the cat. J Physiol (Lond) 342:181–215.

Finkel LH, Edelman GM (1989) Integration of distributed cortical systems by reentry: a computer simulation of interactive functionally segregated visual areas. J Neurosci 9:3188–3208.

Fischer B (1973) Overlap of receptive field centers and representation of the visual field in the optic tract. Vision Res 13:2113–2120.

Gabbott PLA, Somogyi P (1986) Quantitative distribution of GABA-immunoreactive neurons in the visual cortex (area 17) of the cat. Exp Brain Res 61:323–331.

Gilbert C (1977) Laminar differences in receptive field properties of cells in cat primary visual cortex. J Physiol (Lond) 268:391–421.

Gilbert CD (1985) Horizontal integration in the neocortex. Trends Neurosci 8:160–165.

Grigonis AM, Zingaro GJ, Murphy EH (1988) The development of orientation and direction selectivity in the rabbit visual cortex. Develop Brain Res 40:315–318.

Hata Y, Tsumoto T, Sato H, Hagihara K, Tamura H (1988) Inhibition contributes to orientation selectivity in visual cortex of cat. Nature 335:815–817.

Hebb DO (1949) The organization of behavior. New York: Wiley.

Heggelund P (1981) Receptive field organization of simple cells in cat striate cortex. Exp Brain Res 42:89–98.

Heggelund P (1986) Quantitative studies of the discharge fields of single cells in cat striate cortex. J Physiol (Lond) 373:272–292.

Henry GH, Goodwin AW, Bishop PO (1978) Spatial summation of responses in receptive fields of single cells in cat striate cortex. Exp Brain Res 32:245–266.

Hess R, Murata K (1974) Effects of glutamate and GABA on specific response properties of neurones in visual cortex. Exp Brain Res 21: 285–297.

Hochstein S, Shapley RM (1976) Quantitative analysis of retinal ganglion cell classifications. J Physiol (Lond) 262:237–264.

Hodgkin AL, Huxley AF (1952) A quantitative description of membrane current and its application to conduction and excitation in nerve. J Physiol (Lond) 117:500–544.

Hoffmann KP, Stone J, Sherman SM (1972) Relay of receptive-field properties in dorsal lateral geniculate nucleus of cat. J Neurophysiol 35:518–531.

Hopfield JJ (1984) Neurons with graded response have collective computational properties like those of two-state neurons. Proc Natl Acad Sci USA 81:3088–3092.

Hubel DH, Wiesel TN (1961) Integrative action in the cat's lateral geniculate body. J Physiol (Lond) 155:385–398.

Hubel DH, Wiesel TN (1962) Receptive fields, binocular interaction

and functional architecture in the cat's visual cortex. J Physiol (Lond) 160:106–154.
Hubel DH, Wiesel TN (1963) Shape and arrangement of columns in cat's striate cortex. J Physiol (Lond)165:559–568.
Humphrey AL, Sur M, Uhlrich DJ, Sherman SM (1985) Projection patterns of individual X- and Y-cell axons from the lateral geniculate nucleus to cortical area 17 in the cat. J Comp Neurol 233:159–189.
Jones JP, Palmer LA (1987) The two-dimensional spatial structure of simple receptive fields in cat striate cortex. J Neurophysiol 58:1187–1211.
Kammen D, Holmes PJ, Koch C (1989) Cortical architecture and oscillations in neuronal networks: feedback versus local coupling. In: Models of brain function (Cotterill RMJ, ed), pp 273–284. Cambridge: Cambridge UP.
Koch C (1987) A network model for cortical orientation selectivity in cat striate cortex. Invest Ophthalmol Vis Sci 28:126.
Koch C, Poggio T (1987) Biophysics of computation: neurons, synapses, and membranes. In: Synaptic function (Edelman GM, Gall WE, Cowan WM, eds), pp 637–698. New York: Wiley.
Koch C, Douglas R, Wehmeier U (1990) Visibility of synaptically induced conductance changes: theory and simulations of anatomically characterized cortical pyramidal cells. J Neurosci 10:1728–1744.
Linsenmeier RA, Frishman LJ, Jakiela HG, Enroth-Cugell C (1982) Receptive field properties of X and Y cells in the cat retina derived from contrast sensitivity measurements. Vision Res 22:1173–1183.
Martin KAC (1988) From single cells to simple circuits in the cerebral cortex. Q J Exp Physiol 73:637–702.
Martin KAC, Somogyi P, Whitteridge D (1983) Physiological and morphological properties of identified basket cells in the cat's visual cortex. Exp Brain Res 50:193–200.
Miller KD, Keller JB, Stryker MP (1989) Ocular dominance column development: analysis and simulation. Science 245:605–615.
Morrone MC, Burr DC, Maffei L (1982) Functional implications of cross-orientation inhibition of cortical visual cells. I. Neurophysiological evidence. Proc R Soc Lond [Biol] 216:335–354.
Movshon JA, Thompson ID, Tolhurst DJ (1978) Spatial summation in the receptive fields of simple cells in the cat's striate cortex. J Physiol (Lond) 283:53–77.
Nielsen DE (1983) A functional model of the wiring of the simple cells of visual cortex. Biol Cybern 47:213–222.
Orban GA (1984) Neuronal operations in the visual cortex. Berlin: Springer.
Orban GA, Kennedy H, Maes H (1981) Response to movement of neurons in areas 17 and 18. J Neurophysiol 45:1043–1058.
Peichl L, Wässle H (1979) Size, scatter and coverage of ganglion cell receptive field centers in the cat retina. J Physiol (Lond) 291:117–141.
Ramoa AS, Shadlen M, Skottun BC, Freeman RD (1986) A comparison of inhibition in orientation and spatial frequency selectivity of cat visual cortex. Nature 321:237–239.
Richter J, Ullman S (1982) A model for the temporal organization of X- and Y-type receptive fields in the primate retina. Biol Cybern 43:127–145.
Rodieck RW (1965) Quantitative analysis of cat retinal ganglion cell response to visual stimuli. Vision Res 5:583–601.
Sanderson KJ (1971) Visual field projection columns and magnification factors in the lateral geniculate nucleus of the cat. Exp Brain Res 13:159–177.
Sato H, Daw NW, Fox K (1990) Intracellular recording study of stimulus specific response properties in the cat visual cortex. Soc Neurosci Abstr 16:502.6.
Schall JD, Vitek DJ, Leventhal AG (1986) Retinal constraints on orientation specificity in cat visual cortex. J Neurosci 6:823–836.
Schwartz EL (1977) Spatial mapping in the primate sensory projection: analytic structure and relevance to perception. Biol Cybern 25:181–194.
Shapley RM, Lennie P (1985) Spatial frequency analysis in the visual system. Annu Rev Neurosci 8:547–583.
Sherman M (1985) Functional organization of the W-, X- and Y-cell pathways: a review and hypothesis. In: Progress in psychobiology and physiological psychology, Vol 11 (Sprague JM, Epstein AN, eds), pp 233–314. New York: Academic.
Shou T, Leventhal AG (1989) Organized arrangement of orientation-sensitive relay cells in the cat's dorsal lateral geniculate nucleus. J Neurosci 9:4287–4302.
Sillito AM (1975) The contribution of inhibitory mechanisms to the receptive field properties of neurones in the striate cortex of the cat. J Physiol (Lond) 250:305–329.
Sillito AM (1977) Inhibitory process underlying the directional specificity of simple, complex and hypercomplex cells in the cat's visual cortex. J Physiol (Lond) 271:699–720.
Sillito AM (1979) Inhibitory mechanisms influencing complex cell orientation selectivity and their modification at high resting discharge levels. J Physiol (Lond) 289:33–53.
Sillito AM, Kemp JA, Milson JA, Berardi N (1980) A re-evaluation of the mechanisms underlying simple cell orientation selectivity. Brain Res 194:517–520.
Singer W (1977) Effects of monocular deprivation on excitatory and inhibitory pathways in cat striate cortex. Exp Brain Res 134:508–518.
Singer W, Creutzfeldt OD (1970) Reciprocal lateral inhibition of on- and off-center neurones in the lateral geniculate body of the cat. Exp Brain Res 10:311–330.
Skottun B, Bradley A, Sclar G, Ohzawa I, Freeman R (1987) The effects of contrast on visual orientation and spatial frequency discrimination: a comparison of single cells and behavior. J Neurophysiol 57:773–786.
Soodak RE (1987) The retinal ganglion cell mosaic defines orientation columns in striate cortex. Proc Natl Acad Sci USA 84:3936–3940.
Stratford K, Mason A, Larkman A, Major G, Jack J (1989) The modeling of pyramidal neurones in the visual cortex. In: The computing neuron (Durbin R, Miall C, Mitchinson G, eds), pp 296–321. Reading, MA: Addison-Wesley.
Tanaka K (1983) Cross-correlation analysis of geniculostriate neuronal relationships in cats. J Neurophysiol 49:1303–1318.
Tömböl T (1974) An electron microscopic study of the neurons of the visual cortex. J Neurocytol 3:525–531.
Tolhurst DJ, Dean AF (1990) The effects of contrast on the linearity of spatial summation of simple cells in the cat's striate cortex. Exp Brain Res 79:582–588.
Toyama K, Kimura M, Tanaka S (1981) Organization of cat visual cortex as investigated by cross-correlation technique. J Neurophysiol 46:191–201.
Traub RD, Miles R, Wong RKS (1989) Models of the origin of rhythmic population oscillations in the hippocampal slice. Science 243:1319–1325.
Tsumoto T, Eckart W, Creutzfeldt OD (1979) Modification of orientation selectivity of cat visual cortex neurons by removal of GABA mediated inhibition. Exp Brain Res 34:351–363.
Tusa RJ, Palmer LA, Rosenquist AC (1978) The retinotopic organization of area 17 (striate cortex) in the cat. J Comp Neurol 177:213–236.
Vidyasagar TR (1984) Contribution of inhibitory mechanisms to the orientation sensitivity of cat LGN neurones. Exp Brain Res 55:192–195.
Vidyasagar TR (1987) A model of striate response properties based on geniculate anisotrophies. Biol Cybern 57:11–24.
Vidyasagar TR, Urbas JV (1982) Orientation sensitivity of cat LGN neurones with and without inputs from visual cortical areas 17 and 18. Exp Brain Res 46:157–169.
Watkins DW, Berkley MA (1974) The orientation selectivity of single neurons in cat striate cortex. Exp Brain Res 19:433–446.
Wehmeier U, Dong D, Koch C, Van Essen D (1989) Modeling the visual system. In: Methods in neuronal modeling (Koch C, Segev I, eds), pp 335–359. Cambridge: MIT Press.
Wilson HR, Cowan JD (1972) Excitatory and inhibitory interactions in localized populations of model neurons. Biophys J 12:1–24.
Wilson MA, Bower JM (1989) The simulation of large-scale neural networks. In: Methods in neuronal modeling (Koch C, Segev I, eds), pp 291–334. Cambridge: MIT Press.
Winfield DA, Gatter KC, Powell TPS (1980) An electron microscopic study of the types and proportions of neurons in the cortex of the motor and visual areas of the cat and rat. Brain 103:245–258.
Wolf W, Hicks TP, Albus K (1986) The contribution of GABA-mediated inhibitory mechanisms to visual response properties of neurons in the kitten's striate cortex. J Neurosci 6:2779–2795.
Wörgötter F, Eysel UT (1987) Quantitative determination of orientational and directional components in the response of visual cortical cells to moving stimuli. Biol Cybern 57:349–355.
Wörgötter F, Eysel UT (1989) Axis of preferred motion is a function

of bar length in visual cortical receptive fields. Exp Brain Res 76:307–314.

Wörgötter F, Holt G (1991) Spatio-temporal mechanisms in receptive fields of visual cortical simple cells: a model. J Neurophysiol, in press.

Wörgötter F, Gründel O, Eysel UT (1990) Quantification and comparison of cell properties in cat's striate cortex determined by different types of stimuli. Eur J Neurosci 2:928–941.

Wörgötter F, Muche T, Eysel UT (1991a) Correlations between directional and orientational tuning of cells in cat striate cortex. Exp Brain Res, in press.

Wörgötter F, Niebur E, Koch C (1991b) Isotropic connections generate functional asymmetrical behavior in visual cortical cells. J Neurophysiol, in press.